J. Fluid Mech. (1976), *vol.* 74, *part* 3, *pp.* 433–468
Printed in Great Britain

Application of central-limit theorems to turbulence and higher-order spectra

By J. L. LUMLEY
Department of Aerospace Engineering, The Pennsylvania State University
AND K. TAKEUCHI
Department of Civil Engineering, Stanford University

(Received 11 December 1973 and in revised form 6 May 1975)

1. Introduction

In Lumley (1971) a relatively weak form of central-limit theorem was proved for dependent random processes. Much stronger theorems have been in the literature for some time (beginning with Rosenblatt 1956); but the conditions for these theorems (principally, the 'strong-mixing' condition of Rosenblatt), though intuitively appealing, are not directly verifiable in a concrete situation. In addition, the stronger theorems predict more than can be measured. The weak theorem of Lumley (1971) predicts only what can be measured, under conditions that are more easily interpretable and verifiable for turbulence.

Batchelor (1953) was the first to discuss, without proof, the applicability of a central-limit theorem to turbulence problems. Briefly, Batchelor speculated that, if turbulence is a statistically stationary random process, and if segments of finite length are considered in some sense statistically independent, then an integral, being the sum of such segments, should asymptotically have a Gaussian distribution, by the central-limit theorem. In Lumley (1971) higher-order cumulants of integrals were considered, and it was shown that, under certain simple conditions (essentially, the existence of integral scales), the non-dimensional moment ratios must asymptotically approach Gaussian values.

The work presented in this paper began with the idea of testing the results of Lumley (1971) against experimental data. In the course of the investigation, however, it was discovered that the limiting behaviour of the higher-order moments is closely related to the properties of higher-order spectra, which have been a subject of considerable interest among mathematicians in recent years. (See e.g. Rosenblatt 1966; Brillinger & Rosenblatt 1967*a*; Rosenblatt & van Ness 1965.)

There exists, of course, an extensive mathematical literature on second-order spectra of stationary random processes and techniques relating to their estimation. Measurements of second-order spectra associated with turbulent flow are common, so that the nature and behaviour of these spectra are well understood. Despite the recent mathematical interest in higher-order spectra of random processes in the field of turbulence, there is at present no definite application of

higher-order spectra (although the Fourier-transformed Navier–Stokes equation was written in terms of the bispectrum by Yeh & Van Atta 1973). The most closely related work on turbulence is due to Frenkiel & Klebanoff (1967): they investigated properties of higher-order correlations in a turbulent velocity field. Some application of higher-order spectra in the field of oceanography is found in the work of Hasselman, Munk & MacDonald (1963): probabilistic models are used to describe ocean waves and ship motion. This paper stimulated the interest of the mathematical community referred to above.

The purposes of the present paper are thus two: (i) to examine further the central-limit theorem proposed in Lumley (1971), by applying it to turbulence data; (ii) to investigate the higher-order spectra of turbulent flows.

2. Central-limit theorem applied to turbulence

The main argument in Lumley (1971) is as follows. Take $u(t)$, a stationary random variable. If an integral of $u(t)$ over the time interval T is considered, then it is expected that its value will also be a stationary random variable which depends on the origin of the time interval. If the integration time T is large compared with the integral scale $\mathscr{T}$, then the integral can be broken up into sections of length Δ larger than $2\mathscr{T}$, so that the sections are approximately independent. (Cf. Tennekes & Lumley 1972, pp. 213–214.) That is,

$$\int_0^T u(t)\,dt = \int_0^\Delta u(t)\,dt + \int_\Delta^{2\Delta} u(t)\,dt + \dots. \tag{1}$$

As Δ increases, the sections of the integral become more nearly independent, since adjacent sections depend upon each other only near the ends. If the length of each section is Δ, and the total integration time is T, the number of sections is T/Δ.

If matters can be arranged in such a way that both Δ and T/Δ go to infinity as $T \to \infty$, then there will be more and more sections, and they will become less and less dependent, so that the probability distribution of the integral on the left-hand side of (1) may become Gaussian under certain conditions. The conditions to be satisfied by the random process are listed in Lumley (1971). The primary interest relates to the question of whether or not the sections of the integral become independent fast enough for the central-limit theorem to be applied successfully.

If $C_p(T)$ denotes the pth cumulant of $\int_0^T u(t)\,dt$, then it is shown in Lumley (1971) that, if all the moments exist, a necessary and sufficient condition for asymptotic independence of integrals over adjacent segments is

$$\lim_{T\to\infty} C_p(T)/T \to \text{const.} \neq 0, \tag{2}$$

for all p. Satisfaction of (2) for any p assures the Gaussian behaviour of the corresponding moment.†

† Asymptotic independence is not necessary for asymptotic normality, although it is physically most plausible. The necessary and sufficient condition for asymptotic normality is simply $C_p(T)/T^{\frac{1}{2}p} \to 0$, $p > 2$, supposing that $C_2(T)/T \to \text{const.} \neq 0$.

In order to show how fast the integral becomes Gaussian, the quantity expressed by (2) is further investigated. Defining $\mathscr{C}_p$ as the pth cumulant of $u(t)$ at p different times, the left-hand side of (2) is written

$$C_p(T)/T = T^{-1}\int_0^T \overset{p}{\dots} \int_0^T \mathscr{C}_p\, dt_1 \dots dt_p = 2T^{-1}\int_0^T \overset{p-1}{\dots} \int_0^T \int_0^{t_1} \mathscr{C}_p\, dt_1 \dots dt_p$$

$$= 2^{p-1}T^{-1}\int_0^T dt_1 \int_0^{t_1} \overset{p-1}{\dots} \int_0^{t_1} \mathscr{C}_p\, dt_2 \dots dt_p. \tag{3}$$

Using the definition of stationarity, and introducing new variables $t_\alpha - t_1 = x_{\alpha-1}$, (2) becomes

$$\lim_{T\to\infty} \frac{C_p(T)}{T} = 2^{p-1} \underset{[C,1]}{\int_0^\infty} dx_1 \overset{p-1}{\dots} \int_0^\infty dx_{p-1}\, \mathscr{C}_p(x_1, \dots, x_{p-1}). \tag{4}$$

$[C, 1]$ denotes the Cesàro-1 value of the integral. Define an integral scale by

$$\mathscr{T}_p = \left[\underset{[C,1]}{\int_0^\infty} dx_1 \dots \int_0^\infty dx_{p-1} \rho_p(\mathbf{x})\right]^{1/(p-1)}, \tag{5}$$

where $$\rho_p(\mathbf{x}) = \mathscr{C}_p(x_1, \dots, x_{p-1})/\mathscr{C}_p(0).$$

Then (4) is written as

$$C_p(T)/T \to 2^{p-1}\mathscr{T}_p^{p-1}\mathscr{C}_p(0). \tag{6}$$

Thus, for a process whose moments exist, a sufficient condition for Gaussian behaviour of the pth moment is the existence ($\neq 0$) of the pth-order integral scale. Using the relation $C_2(T) \to 2\mathscr{C}_2(0)\, T\mathscr{T}_2$, an alternative form of (6) is given in Lumley (1971):

$$\frac{C_p(T)}{C_2(T)^{\frac{1}{2}p}} \to \mathscr{C}_p(0)\,[\mathscr{C}_2(0)]^{-\frac{1}{2}p}\left[\frac{2\mathscr{T}_2}{T}\right]^{\frac{1}{2}p-1}\left[\frac{\mathscr{T}_p}{\mathscr{T}_2}\right]^{p-1}. \tag{7}$$

For $p = 4$, (7) becomes

$$\frac{C_4(T)}{[C_2(T)]^2} \to \frac{\mathscr{C}_4(0)}{[\mathscr{C}_2(0)]^2}\frac{2\mathscr{T}_2}{T}\left(\frac{\mathscr{T}_4}{\mathscr{T}_2}\right)^3 \quad \text{or} \quad K_x - 3 \to (K_u - 3)\frac{2\mathscr{T}_2}{T}\left(\frac{\mathscr{T}_4}{\mathscr{T}_2}\right)^3. \tag{8}$$

K_x and K_u are the kurtosis of $x = \int_0^T u(t)\, dt$ and $u(t)$, respectively. Equation (8) says in essence that the variable x behaves like a Gaussian variable in terms of its fourth moment as $T \to \infty$, and the rate of approach is inversely proportional to the integration time T.

The above analysis was applied in Lumley (1971) to the 'weak interaction' hypothesis introduced by Kraichnan (1959). The essential qualitative content of this hypothesis is that the effective dynamical coupling and statistical interdependence, among any few individual Fourier amplitudes corresponding to different wave vectors, are very weak. The substantial departure from normality of the velocity distribution in a turbulent field appears as the summed effect of very many of these very weak statistical dependences. Simply stated, the hypothesis is that the narrow-band filtered Fourier coefficients actually become statistically independent of each other asymptotically as the bandwidth goes to zero.

Since a narrow-band filtered Fourier coefficient of bandwidth $\Delta\omega$ is (proportional to) the integral over an increasing interval $T = 1/\Delta\omega$ of $u(t)\exp(i\omega t)$, we may expect to be able to apply the above reasoning to this case. Rewriting (8), we would have

$$K(\Delta\omega) - 3 = [K(\infty) - 3][2\mathscr{T}_2\Delta\omega](\mathscr{T}_4/\mathscr{T}_2)^3. \tag{9}$$

$\mathscr{T}_2$ is the integral scale defined from the spectrum, i.e.

$$\mathscr{T}_2 = \pi S(\omega)/\overline{u^2}.$$

The expression given in (9) is the form to which the data is applied in this work. The fact that $u(t)\exp(i\omega t)$ is both complex and only second-order stationary will introduce some analytical complications, which are not of a serious nature. The experimental results thus serve to verify both the theorem and the weak interaction hypothesis.

3. Higher-order spectra

The representative forms of the quantity $C_p(T)$ may be written

$$\left.\begin{aligned} C_2(T) &= \iint_0^T E\{u(t)\,u(t')\}\,dt\,dt' = 2E\{u^2\}T\int_0^T (1 - t/T)\,R(t)\,dt \\ &= \iint_0^T \mathscr{C}_2(t,t')\,dt\,dt', \\ C_3(T) &= \iiint_0^T E\{u(t)\,u(t')\,u(t'')\}\,dt\,dt'\,dt'' = \iiint_0^T \mathscr{C}_3(t,t',t'')\,dt\,dt', \\ C_p(T) &= \int_0^T \overset{p}{\cdots} \int_0^T \mathscr{C}_p(t_1,\ldots,t_\alpha,\ldots,t_p)\,dt_1\,dt_2,\ldots,dt_p. \end{aligned}\right\} \tag{10}$$

The most convenient extension of the second-order autocorrelation $R(t) \equiv \mathscr{C}_2(t)$ to higher orders is the cumulant $\mathscr{C}_p(t_1,\ldots,t_p)$, rather than the moment of order p. This is because, for $p > 3$, there are in general directions in the hyper-space of the moment along which the moment does not vanish, even if the random function is asymptotically statistically independent of itself at large separations. In the cumulant, on the other hand, just this part is subtracted, so that (in the case of asymptotic independence) the cumulant will vanish in all (hyper) directions.

As is well known, the second-order spectrum is defined in terms of the correlation function as

$$S(\omega) = \frac{1}{2\pi}\int_{-\infty}^{+\infty} \exp(-i\omega\tau)\,R(\tau)\,d\tau. \tag{11}$$

Designate $S(\omega)$ by $S_2(\omega)$, and write

$$S_2(\omega) = \frac{1}{2\pi}\int_{-\infty}^{+\infty} \exp(-i\omega\tau)\,\mathscr{C}_2(\tau)\,d\tau. \tag{12}$$

Then, in a similar manner, it might be suspected that spectra higher than second order may be defined, using higher-order cumulants, as

$$S_p(\omega_1, \omega_2, \ldots, \omega_{p-1}) = \frac{1}{(2\pi)^{p-1}} \int_{-\infty}^{\infty} \cdots \int_{p-1}^{\infty} \exp\left[-i(\omega_1\tau_1 + \omega_2\tau_2 + \ldots + \omega_{p-1}\tau_{p-1})\right] \times \mathscr{C}_p(\tau_1, \ldots, \tau_{p-1})\, dt_1 \ldots dt_{p-1}. \quad (13)\dagger$$

Formal definitions (with conditions for existence, etc.), corresponding to (13), were given by Brillinger & Rosenblatt (1967 *a*), who also discussed (1967 *b*) convergence of estimates for these higher-order spectra. This discussion of convergence has many points of similarity with the analysis given here. If we take the case of $p = 4$ in (13), the fourth-order spectrum is defined by

$$S_4(\omega_1, \omega_2, \omega_3) = \frac{1}{(2\pi)^3} \iiint_{-\infty}^{+\infty} \exp\left[-i(\omega_1 x_1 + \omega_2 x_2 + \omega_3 x_3)\right] \mathscr{C}_4(x_1, x_2, x_3)\, dx_1\, dx_2\, dx_3. \quad (14)$$

In § 2 we suggested that, for narrow-band filtered Fourier coefficients, the rate at which they approach Gaussian behaviour might be given by

$$K(\Delta\omega) - 3 \cong [K(\infty) - 3]\,[2\mathscr{T}_2 \Delta\omega]\,[\mathscr{T}_4/\mathscr{T}_2]^3.$$

Here,

$$\Delta\omega = \frac{1}{T}, \quad \mathscr{T}_2 = \frac{\pi}{2\sigma^2} S_2(\omega), \quad \sigma^2 = \int_0^{\infty} S_2(\omega)\, d\omega,$$

$$\mathscr{T}_4 \sim \left[\iiint_0^{\infty} \mathscr{C}_4(x_1, x_2, x_3)\, dx_1\, dx_2\, dx_3\right]^{\frac{1}{3}}.$$

Equation (9) can be rewritten as

$$\frac{1}{64} \frac{T}{\pi[K(\infty) - 3]} [K(\Delta\omega) - 3] \sim \frac{1}{(2\pi)^3 S_2^2(\omega)} \mathscr{T}_4^3, \quad (15)$$

where some of the quantities are not yet well-defined. Now, let us consider the Fourier coefficients, defined as

$$X(\omega) = \int_0^T u(t) \exp(-i\omega t)\, dt, \quad v(t) = u(t) \exp(-i\omega t).$$

The variable $v(t)$, defined this way, is only second-order stationary, and is in addition complex. Hence, it is not immediately clear what form the fourth moment should take. A careful analysis will be carried out in § 7.2. For now, we shall use the result obtained there:

$$\tfrac{1}{2}((\overline{\mathrm{Re}\, X})^4 - 3(\overline{\mathrm{Re}\, X})^{2^2} + (\overline{\mathrm{Im}\, X})^4 - 3(\overline{\mathrm{Im}\, X})^{2^2}) \sim 2^3 T \iiint_{\substack{0 \\ [C,1]}}^{\infty} \mathscr{C}_4(\mathbf{x}) [\tfrac{1}{2} \cos\omega x_1 \cos\omega x_2 \cos\omega x_3 - \tfrac{1}{8} \cos\omega(x_1 + x_2 + x_3)]\, d\mathbf{x}. \quad (16)$$

† Although $\mathscr{C}_p$ appears to be a function of $t_1, \ldots, t_p$, in fact stationarity implies that it is a function of only $p-1$ differences. We shall consciously abuse notation somewhat by using the same letter $\mathscr{C}_p$ to indicate the function of $t_1, \ldots, t_p$ and the function of the differences $\tau_1, \ldots, \tau_{p-1}$.

We shall take the normalized left-hand side of (16) as our definition of the excess of the Fourier coefficients:

$$K(\Delta\omega)-3 \equiv \frac{\overline{(\mathrm{Re}\,X)^4}-3\overline{(\mathrm{Re}\,X)^2}^2+\overline{(\mathrm{Im}\,X)^4}-3\overline{(\mathrm{Im}\,X)^2}^2}{\overline{(\mathrm{Re}\,X)^2}^2+\overline{(\mathrm{Im}\,X)^2}^2}.$$

The expression (16) is clearly proportional to a particular part of the fourth-order spectrum given by (14), and will be examined further in § 7.2. Evidently,

$$\mathscr{T}_4^* = \left[\iiint_{\substack{0\\[C,\,1]}}^{\infty} \mathscr{C}_4(x_1,x_2,x_3)\{\tfrac{1}{2}\cos\omega x_1\cos\omega x_2\cos\omega x_3 - \tfrac{1}{8}\cos\omega(x_1+x_2+x_3)\}\,dx_1\,dx_2\,dx_3\right]^{\frac{1}{3}}$$

is the proper expression for the higher-order integral scale $\mathscr{T}_4$ of the random variable $v(t)$. Thus, using this, (15) becomes

$$\frac{1}{64}\frac{T}{\pi(K(\infty)-3)}[K(\Delta\omega)-3] \sim \frac{1}{(2\pi)^3 S_2^2(\omega)} \times \iiint_{\substack{0\\[C,\,1]}}^{\infty} \mathscr{C}_4(\mathbf{x})\{\tfrac{1}{2}\cos\omega x_1\cos\omega x_2\cos\omega x_3 - \tfrac{1}{8}\cos\omega(x_1+x_2+x_3)\}\,dx_1\,dx_2\,dx_3. \quad (17)$$

The right-hand side of (17) is now properly normalized. We shall take it as the definition of that certain part (referred to above, and yet to be identified) of the fourth-order cumulant spectrum which we designate by $S_4(\omega)$. Thus,

$$\frac{1}{64}\frac{T}{\pi[K(\infty)-3]}[K(\Delta\omega)-3] = \frac{S_4(\omega)}{S_2^2(\omega)}. \quad (18)$$

4. Data acquisition

The non-Gaussian data were obtained in open jet turbulence, and in a simple pipe-flow turbulence. The purpose of collecting the data in two different turbulent flows was to examine the effect of the scales involved in each of the flows on the rate of convergence to Gaussian of the variables. The range of scales available in a turbulent flow is monotone in the turbulent Reynolds number (based, say, on r.m.s. fluctuating velocity and Taylor microscale). Consequently, two flows were selected with widely-differing Reynolds numbers. The estimated turbulence Reynolds number for the jet flow is 670, and that of the pipe flow is estimated to be 55.

4.1. *Jet turbulence*

The jet turbulence signals were obtained in the high-shear mixing layer of an axi-symmetric jet. The jet facility used for the acquisition of the data was originally designed and constructed by Nilsen (1969), and is at the Garfield Thomas Water Tunnel of the Applied Research Laboratory of The Pennsylvania State University. The details of this facility, and the turbulence characteristics of the flow, can be found in Nilsen (1969) and Von Frank (1970). Briefly, a standard

screened plenum and contraction produce a parallel uniform, low-turbulence flow at $30\,\mathrm{m\,s^{-1}}$, which exits horizontally from a 0·3 m diameter hole in a large baffle plate.

The point in the flow field selected for the measurements was six jet diameters downstream, and one half jet diameter radially outwards in the horizontal. According to the data obtained by Nilsen (1969), this measurement position is just beyond the extent of the potential core region in the downstream direction.

Several characteristics of the turbulence were measured prior to recording the turbulent velocity and velocity derivative signals on a magnetic tape. The turbulence intensity $(\overline{u^2})^{\frac{1}{2}}/U$ at the measuring position was found to be 0·149, based on the exit velocity. The Taylor microscale λ was found to be 0·212 cm. It was obtained from

$$\lambda = \overline{(u^2)}^{\frac{1}{2}}[\overline{(\partial u/\partial x)^2}]^{-\frac{1}{2}}. \tag{19}$$

The mean-square spacewise derivative was obtained from the time derivative, using Taylor's hypothesis:

$$\partial u/\partial t = -U\,\partial u/\partial x.$$

For the measurements of velocity and its time derivative, a constant-temperature hot-wire anemometer, originally designed by Lumley & Wyngaard (1967), was used in conjunction with a Disa 55D10 linearizer. An overheat ratio of 0·8 and a linearizer exponent setting of 1·8 were found to yield a linear calibration curve. The linearizer output was fed to a Butterworth filter–differentiator (Wyngaard & Lumley 1967). The latter has a pure amplifier, and a low-pass filter with the added capability of differentiation. The output of the filter–differentiator was then essentially proportional to either the streamwise velocity fluctuation or its time derivatives. The final signals were recorded simultaneously in FM mode at 30 i.p.s. on a Pemco recorder. The total record of data obtained was approximately 300 s. The hot wire used in this measurement was a silver Wollaston, with diameter 1·27 μm, a span of 1·8 mm between supports, and an etched length of approximately 0·7 mm.

4.2. *Pipe-flow turbulence*

The experimental set-up for pipe-flow turbulence can be achieved with ease, another reason for selecting this particular flow. The mean velocity selected for the flow was $7{\cdot}6\,\mathrm{m\,s^{-1}}$; and the pipe diameter was 2·54 cm. The corresponding Reynolds number, based on pipe diameter, was $1{\cdot}2 \times 10^4$. The length of the pipe was 1·5 m, or approximately 60 diameters. The turbulence intensity was approximately 3 % at the measuring position at the exit.

The inlet end of the pipe was connected to a centrifugal blower via a flexible hose, to eliminate possible vibration from the motor. The hot wire used was the same as that used in the measurement of jet turbulence (diameter 1·27 μm, etched length 0·7 mm). The measuring position was approximately one half-radius from the centre-line.

The turbulence signal was obtained using the same constant-temperature anemometer. The linearizer was deemed unnecessary, because of the low turbulence intensity of the flow. The output signal from the anemometer was then

passed through the Butterworth filter–differentiator, to the Pemco tape recorder. The differentiated velocity signals were recorded in FM mode on four of its channels. Each channel was recorded separately: i.e. after recording each, the tape was rewound and the next recorded. This procedure was repeated until all the four were filled. This gave four channels of independent data, a total record length of approximately 1200 s.

5. Data processing

The data were processed by a Pastoriza analog-to-digital converter. The result was Fourier transformed. The procedures of conversion and Fourier transformation were very similar to those described by Takeuchi & Lumley (1976).

For jet flow, the highest frequency present in the data was found to be 14 kHz; thus, a sampling rate of 36 000 samples s^{-1} was chosen for this flow. The fundamental frequency (minimum filter bandwidth) Δf selected was approximately 4·4 Hz. The corresponding number of data points in a given block to achieve this frequency resolution was $N = 8192$ points. For pipe flow, the spectrum band was found to be 7 kHz; thus a rate of 18 000 samples s^{-1} was chosen. The fundamental frequency (filter bandwidth) chosen was 17·57 Hz, the corresponding number of data points in one block being $N = 1024$.

In estimating the adequacy of the fundamental frequency (alternatively, the bandwidth of the filter), the integral scale of the flow was estimated on the basis of the geometrical scale involved. Let the integral scale be estimated by $\mathscr{T} \sim \mathscr{L}/U$ s, where $\mathscr{L}$ is the characteristic length and U is the mean flow velocity. Then, for the jet flow, $\mathscr{L} \sim 0{\cdot}3$ m, $U \sim 18$ m s^{-1} and $\mathscr{T} \sim \frac{1}{60}$ s. This integral scale with the bandwidth resolution (Δf) of approximately 4 Hz will give a product $\Delta f \mathscr{T} \sim \frac{1}{15}$. In pipe flow, the characteristic length $\mathscr{L}$ is approximately 2·54 cm, and with mean flow velocity of $U = 7{\cdot}6$ m s^{-1}, we obtain $\mathscr{T} \sim \frac{1}{300}$ s. Were approximately the same bandwidth resolutions desired in the pipe flow as in the jet flow, a bandwidth of $\Delta f = 20$ Hz would be sufficient to give a product $\Delta f \mathscr{T} \sim \frac{1}{15}$. Thus, the selected bandwidth of 17·57 Hz has approximately the same bandwidth resolution as the jet flow, or better.

A preliminary statistical analysis of the digitized data was performed, which included probability densities and spectra. (The methods of computation are described in Takeuchi & Lumley 1976.) The Fourier-transformed data were digitally filtered, and the filtered Fourier coefficients analysed statistically.

In the investigation of the filtered Fourier coefficients, the filter bandwidth was formed as follows. Let Δf be the fundamental filter bandwidth with centre frequency at f_0. Then the following bandwidths correspond to the frequencies written beside them:

$$\left.\begin{aligned} &1\Delta f, \quad A(f_0); \\ &2\Delta f, \quad \tfrac{1}{2}A(f_0-\Delta f)+A(f_0)+\tfrac{1}{2}A(f_0+\Delta f); \\ &3\Delta f, \quad A(f_0-\Delta f)+A(f_0)+A(f_0+\Delta f); \\ &4\Delta f, \quad \tfrac{1}{2}A(f_0-2\Delta f)+A(f_0-\Delta f)+A(f_0)+A(f_0+\Delta f)+\tfrac{1}{2}A(f_0+2\Delta f). \end{aligned}\right\} \tag{20}$$

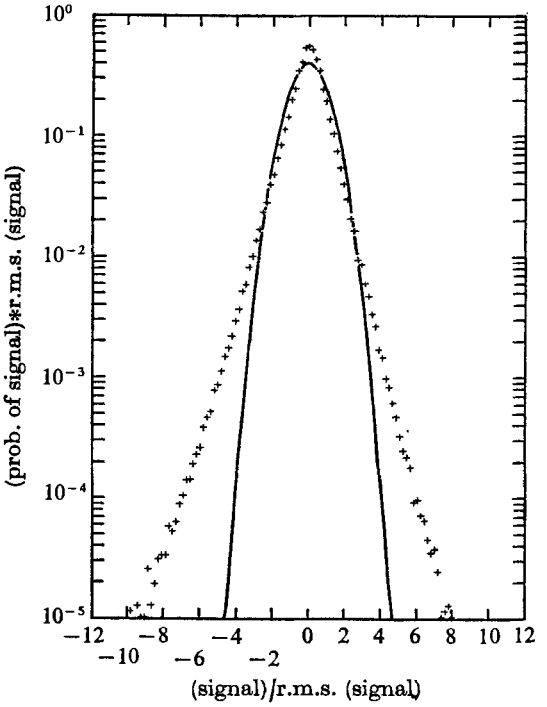

FIGURE 1. Probability density of Du/Dt for jet flow. +, experimental data. ——, Gaussian.

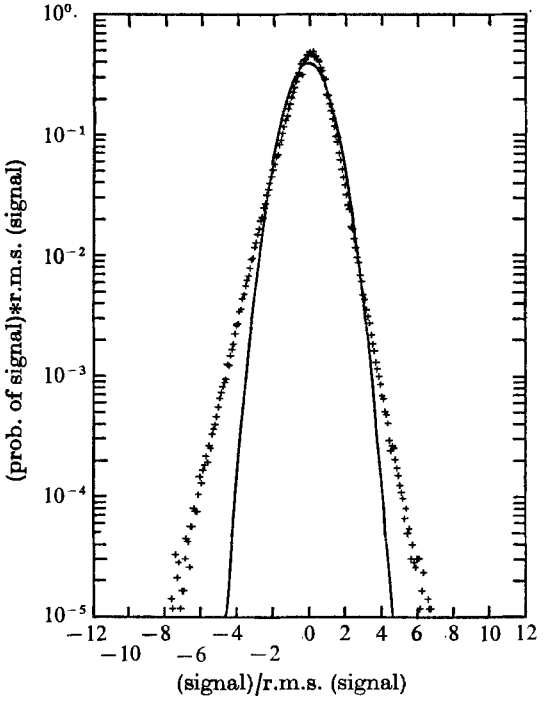

FIGURE 2. Probability density of Du/Dt for pipe flow. +, experimental data. ——, Gaussian.

This method of filtering was applied to both the real and imaginary part of the Fourier coefficients. The statistical analyses of the resulting filtered coefficients were performed separately for the real and imaginary part of the coefficient, and the final values of the moment were obtained by taking the average of the two parts. The number of data used in the actual calculations of kurtosis for amplitude statistics were: for jet flow, 1250 records of 8192 data points per record; for pipe flow, 20 000 records of 1024 data points per record. Thus, for the statistics of the filtered Fourier coefficients, the pipe flow had 20 000 data points, while jet flow used 1250 data points for each bandwidth.

6. Characteristics of data

Figure 1 represents the normalized probability density of the jet turbulence derivative signal. The solid curve represents the Gaussian density with the same mean standard deviation as the turbulence signal. The probability density in figure 1 was obtained using a 4×10^6 data set. Figure 2 is a similar plot for the turbulence derivative signal of pipe flow. The probability density in figure 2 is based on a data set size of 5×10^6 points. Figures 1 and 2 show that the experimental results are slightly skewed to the negative side, as they should be, and do not become seriously non-Gaussian until a signal to r.m.s. (signal) ratio of three. Thus, the fact that the turbulence derivative signal is not Gaussian cannot be seen in the probability density plot, unless proper care is taken to cover more than three times the standard deviation in the digital processing. The results of the amplitude statistics gave a skewness (non-dimensionalized third moment) of $-0{\cdot}337$, and a kurtosis (non-dimensionalized fourth moment) of 6·32 for jet turbulence, and a skewness of $-0{\cdot}399$ and a kurtosis of 4·74 for the pipe turbulence.

Figures 3 and 4 represent velocity spectra of jet and pipe turbulence, respectively. The plots were normalized so that

$$\int_0^\infty \frac{(\kappa\eta)^2 F(\kappa)}{(\epsilon\nu^5)^{\frac{1}{4}}}\, d(\kappa\eta) = \tfrac{1}{15}.$$

This is a consequence of the definition of the one-dimensional velocity spectrum $F(\kappa)$ and the isotropic relation

$$\epsilon = 15\nu\overline{(\partial u/\partial x)^2}.$$

η is the Kolmogoroff microscale

$$\eta = (\nu^3/\epsilon)^{\frac{1}{4}}.$$

ν is the kinematic viscosity. The values of η were found to be 0·04 mm for the jet flow, and 0·17 mm for pipe flow.

Figures 5 and 6 are the similar plots for derivative signals. By use of figures 3 and 4, the universal constant defined by α in $F(\kappa) = \alpha\epsilon^{\frac{2}{3}}\kappa^{-\frac{5}{3}}$, for $\kappa\eta \ll 1$, is found to be $\alpha \sim 0{\cdot}53$ for jet flow and $\alpha \sim 0{\cdot}57$ for the pipe flow. These values of α lie well within the range of values reported by other workers.

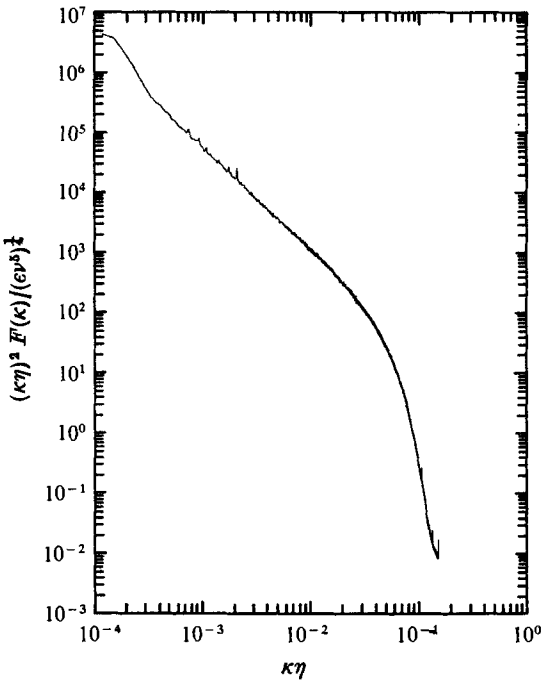

FIGURE 3. Kolmogorov plot of velocity spectrum for jet flow.

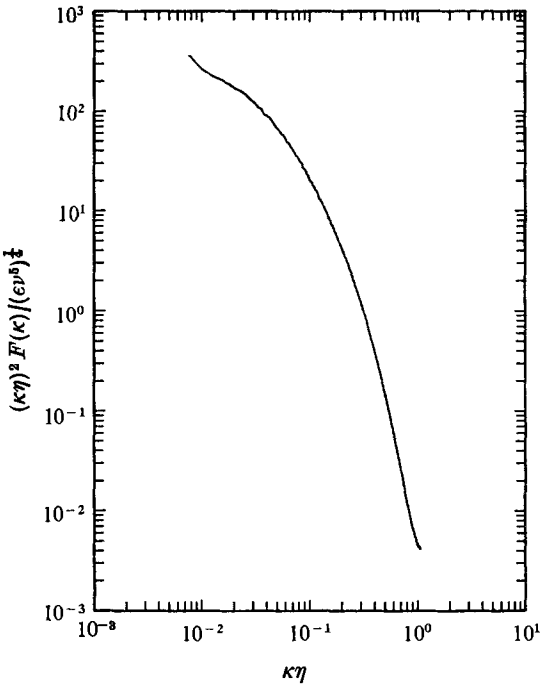

FIGURE 4. Kolmogorov plot of velocity spectrum for pipe flow.

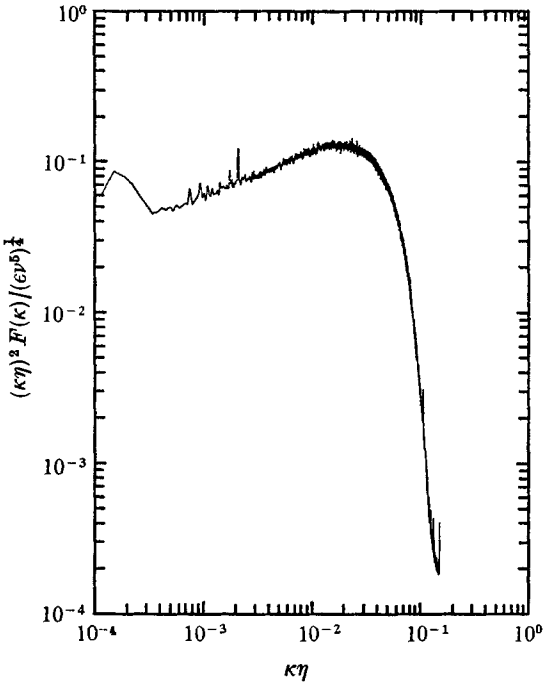

FIGURE 5. Kolmogorov plot of dissipation spectrum for jet flow.

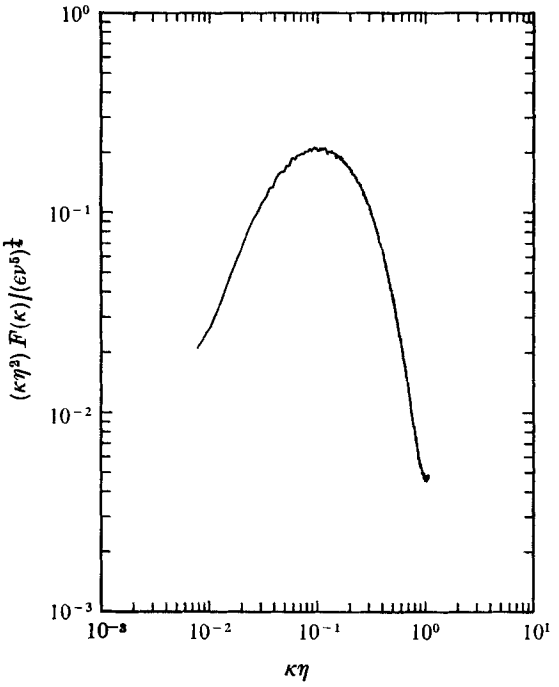

FIGURE 6. Kolmogorov plot of dissipation spectrum for pipe flow.

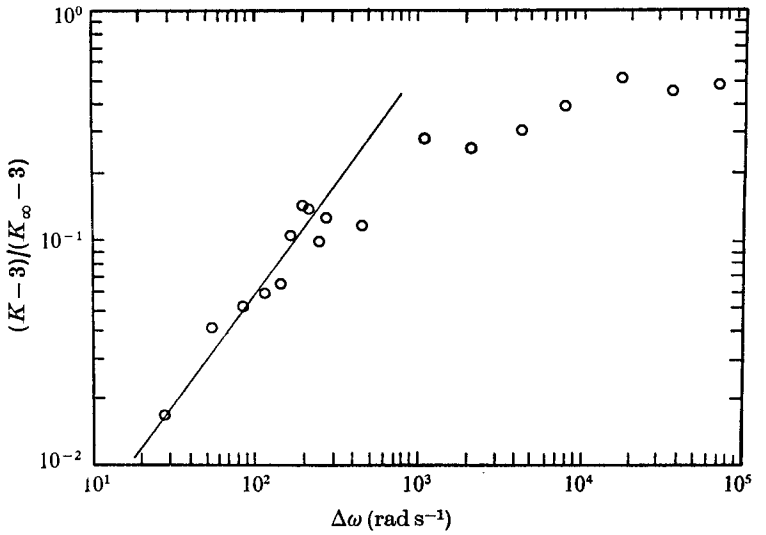

FIGURE 7. Kurtosis of narrow-band filtered velocity derivative for jet flow.

7. Results and discussion

7.1. *Central-limit theorem*

In § 3 it was shown that, under appropriate conditions, the narrow-band averaged Fourier coefficients of dependent random variables become Gaussian, and statistically independent of each other asymptotically as the bandwidth goes to zero ('weak interaction'). Taking as evidence of the approach to Gaussian behaviour the approach of the kurtosis of the process to three, the relation given by (9) was obtained. The validity of this expression was examined using the data obtained in this investigation.

Figure 7 is the result obtained for jet flow at a centre-frequency of 5·8 kHz and a minimum bandwidth of 4·39 Hz; the corresponding bandwidth to centre-frequency ratio was 7×10^{-4}. The slope is clearly tending toward one, as predicted. The constant in (9) is evidently close to 10^2, so that $\mathscr{T}_4/\mathscr{T}_2 \sim 4{\cdot}65$. The value of the integral scale calculated from

$$\mathscr{T}_2 = \pi S(\omega)/\overline{u^2}$$

was $4{\cdot}78 \times 10^{-5}$ s, which gives $\mathscr{T}_4 \sim 1{\cdot}94 \times 10^{-4}$ s. The integral scale of velocity itself $\mathscr{T}_u$ calculated from the normalized spectrum is $9{\cdot}26 \times 10^{-3}$ s. (For the method of calculation, see Lumley 1970.) This gives a ratio of $\mathscr{T}_u/\mathscr{T}_4 \sim 47{\cdot}8$. The length of record used in the calculation was approximately 284 s, which corresponds to roughly $7 \times 10^6 \mathscr{T}_2$.

Figure 8 represents the result of the computation for the pipe-flow turbulence. The slope is also clearly tending toward one. The constant $\beta = (\mathscr{T}_4/\mathscr{T}_2)^3$ in this case is apparently close to 10; the ratio $\mathscr{T}_4$ to $\mathscr{T}_2$ is then 2·16. The $\mathscr{T}_2$ calculated was $5{\cdot}5 \times 10^{-5}$ s so that $\mathscr{T}_4 \sim 1{\cdot}18 \times 10^{-4}$ s. The integral scale of velocity was $1{\cdot}44 \times 10^{-3}$ s; this yields $\mathscr{T}_u/\mathscr{T}_4 \sim 12{\cdot}2$. The fundamental bandwidth (Δf) chosen

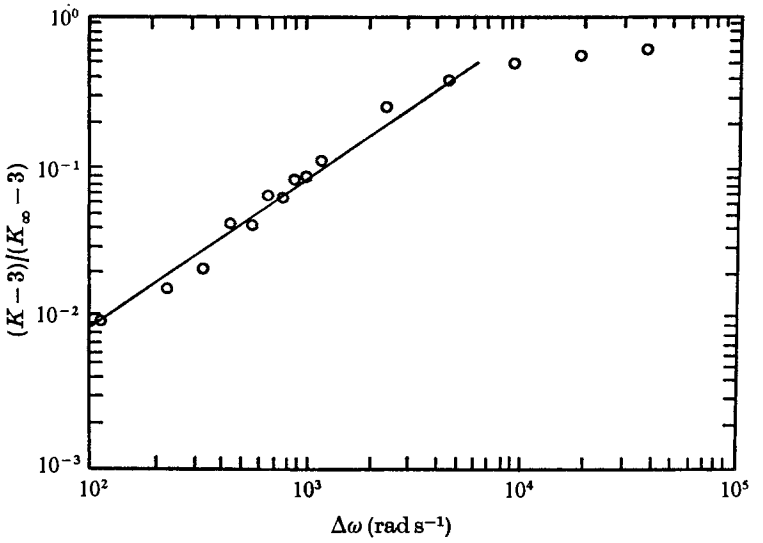

FIGURE 8. Kurtosis of narrow-band filtered velocity derivative for pipe flow.

was 17·57 Hz, and the centre-frequency was 3·00 kHz. The corresponding bandwidth to centre-frequency ratio is $5{\cdot}86 \times 10^{-3}$.

The length of the record used in this calculation was 1142 s, which corresponds to $2{\cdot}08 \times 10^7 \mathscr{T}_2$. This long record of available data is responsible for the smoothness of the curve shown in figure 8. It must be pointed out here, by comparing figures 7 and 8, that the convergence of the variables to the Gaussian is approximately a factor of two better for the results shown in figure 8 (pipe flow) than for those shown in figure 7 (jet flow).

The bandwidth resolution with respect to the integral scale of the process can be expressed by the product of the fundamental bandwidth Δf and an integral scale $\mathscr{T}$; and it is desirable to have this product small, in order to achieve convergence of the variable to Gaussian. Because the process considered in this study is that obtained from the velocity derivatives, an intuitive choice of the integral scale to be used in forming the product is $\mathscr{T}'_u$, or the scale associated with the derivatives. (See Lumley 1970.) The calculated result of the product for each flow used in this study is: for jet flow, $\Delta f \mathscr{T}'_u \sim 3{\cdot}1 \times 10^{-4}$; for pipe flow, $\Delta f \mathscr{T}'_u \sim 2 \times 10^{-3}$. Examination of these results indicates that the values of the product $\Delta f \mathscr{T}'_u$ do not reflect the behaviour of the filtered signals shown in figures 7 and 8. As was pointed out, the convergence of the variable shown in figure 8 is a factor of more than two better than that shown in figure 7. This implies that the values of the product $\Delta f \mathscr{T}$ should be approximately a factor of two smaller in the pipe flow than in the jet flow.

This suggests that the integral scale $\mathscr{T}'_u$ is not the proper one to be used in forming the product of $\mathscr{T}$; and it is necessary to examine the possibility of using other integral scales in describing the bandwidth resolution. The candidates for relevant integral scales in this particular study are: $\mathscr{T}'_u, \mathscr{T}_u, \mathscr{T}_4$, or that of velocity

		Jet	Pipe
Δf		4·4	17·5
Δf/c.f.		7×10^{-4}	$5{\cdot}8 \times 10^{-3}$
$\mathscr{T}_4/\mathscr{T}_2$		4·65	2·16
$\mathscr{T}_2$		$4{\cdot}2 \times 10^{-5}$	$5{\cdot}5 \times 10^{-5}$
$\mathscr{T}_4$		$1{\cdot}9 \times 10^{-4}$	1.2×10^{-4}
$\mathscr{T}'_u$		7×10^{-5}	$1{\cdot}15 \times 10^{-4}$
$\mathscr{T}_u$		$9{\cdot}2 \times 10^{-3}$	$1{\cdot}4 \times 10^{-3}$
$\mathscr{T}_u/\mathscr{T}_4$		47·8	12·2
Record length	$\mathscr{T}'_u$	7×10^6	2×10^7
	$\mathscr{T}_u$	$3{\cdot}1 \times 10^4$	$8{\cdot}2 \times 10^5$
	$\mathscr{T}_4$	$1{\cdot}5 \times 10^6$	$9{\cdot}5 \times 10^6$
	s	284	1142
Record		1250	20000
$\Delta f\mathscr{T}'_u$		$3{\cdot}1 \times 10^{-4}$	2×10^{-3}
$\Delta f\mathscr{T}_u$		4×10^{-2}	$2{\cdot}4 \times 10^{-2}$
$\Delta f\mathscr{T}_4$		$8{\cdot}4 \times 10^{-4}$	2×10^{-3}

TABLE 1. Comparison of integral scales

derivatives, the velocity, and the scales associated with the fourth moment, respectively.

Table 1 is a summary of various quantities of significance in the study of the narrow-band filtered signals, expressed in terms of the integral scales above. Table 1 indicates that the proper integral scale to be used in the description of the bandwidth resolution must be that of velocity itself, or $\mathscr{T}_u$. The product $\Delta f\mathscr{T}_u$ shown in table 1 is approximately a factor of two smaller in pipe flow than in jet flow. It seems appropriate to conclude that the bandwidth resolution $\Delta f\mathscr{T}_u$ required to achieve convergence of variables to the Gaussian is of order 10^{-2}.

It is not too surprising to find that the relevant integral scale for the bandwidth resolution is $\mathscr{T}_u$, not $\mathscr{T}'_u$, even though the process under consideration is the derivative signal; for the high frequencies in turbulence are known to be modulated by the frequencies corresponding to the energy-containing eddies; so the longest time scale present will still be that of the latter. This modulation by larger scales is of course responsible for the intermittency of the small scales. (See e.g. Novikov & Stewart 1964.) The intermittency is in turn responsible for the non-Gaussian behaviour. The argument of Lumley (1970), suggesting the relevance of T'_u, is based on properties of Gaussian processes, which have little bearing on turbulence.

Figures 9–13 show that the filtered Fourier coefficients approach a Gaussian distribution as the bandwidth of the filter becomes small. The probability densities shown in these figures were calculated with a 2×10^5 data set. The approach to a Gaussian distribution of the coefficient is clear.

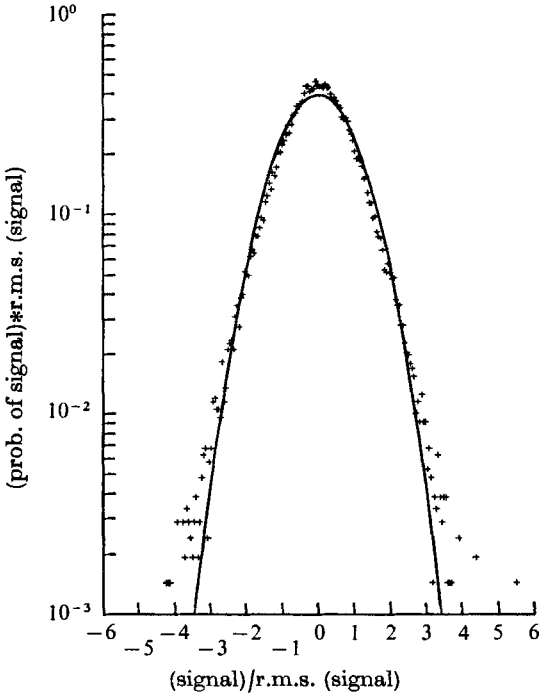

FIGURE 9. Probability density of filtered Fourier coefficients of Du/Dt for pipe flow. Bandwidth $80\Delta f$ ($1\Delta f$ = 17·57 Hz). +, experimental data. ——, Gaussian.

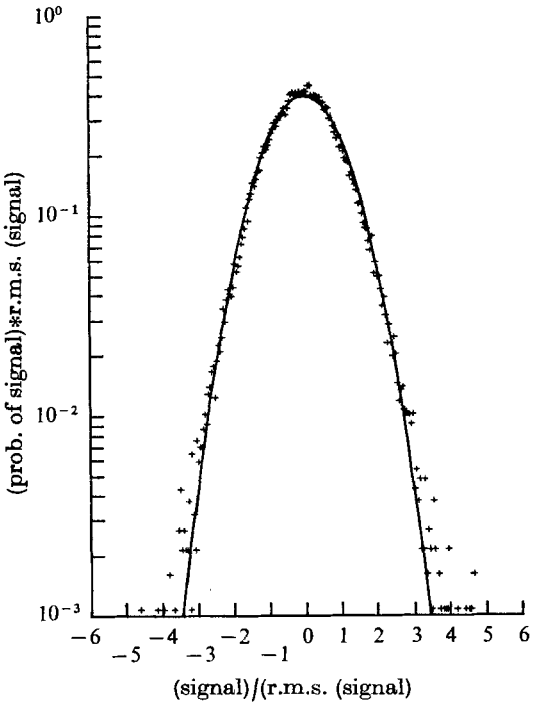

FIGURE 10. Probability density of filtered Fourier coefficients of Du/Dt for pipe flow. Bandwidth $20\Delta f$ ($1\Delta f$ = 17·57 Hz). +, experimental data. ——, Gaussian.

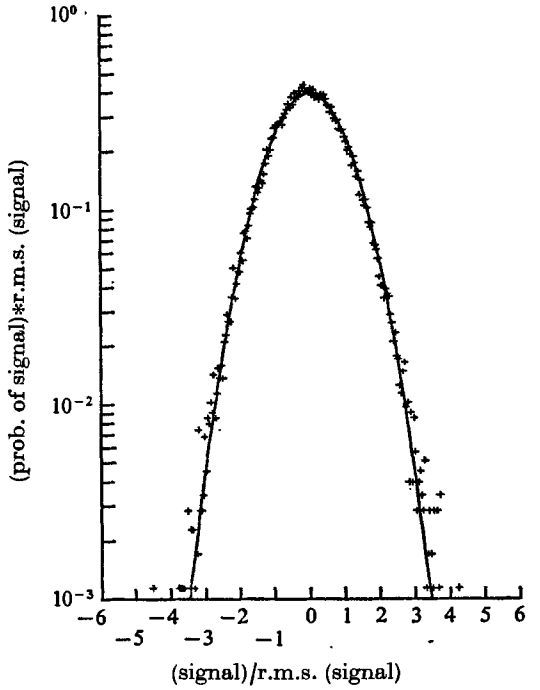

FIGURE 11. Probability density of filtered Fourier coefficients of Du/Dt for pipe flow. Bandwidth $9\Delta f$ ($1\Delta f$ = 17·57 Hz). +, experimental data. ——, Gaussian.

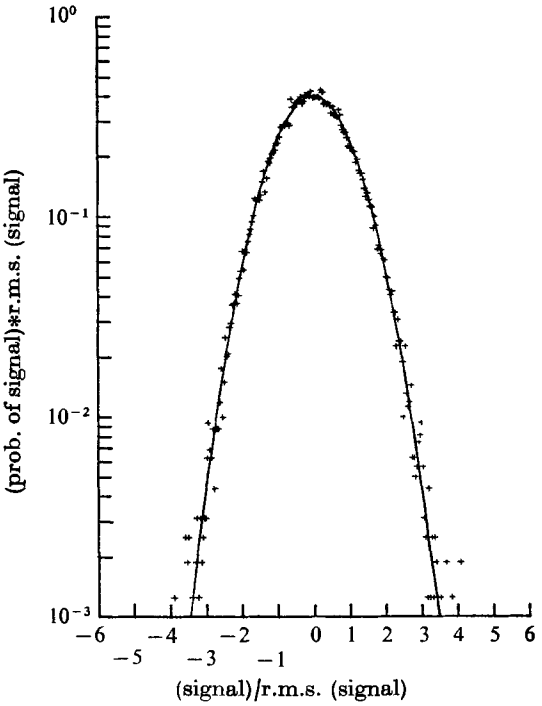

FIGURE 12. Probability density of filtered Fourier coefficients of Du/Dt for pipe flow. Bandwidth $5\Delta f$ ($1\Delta f$ = 17·57 Hz). +, experimental data. ——, Gaussian.

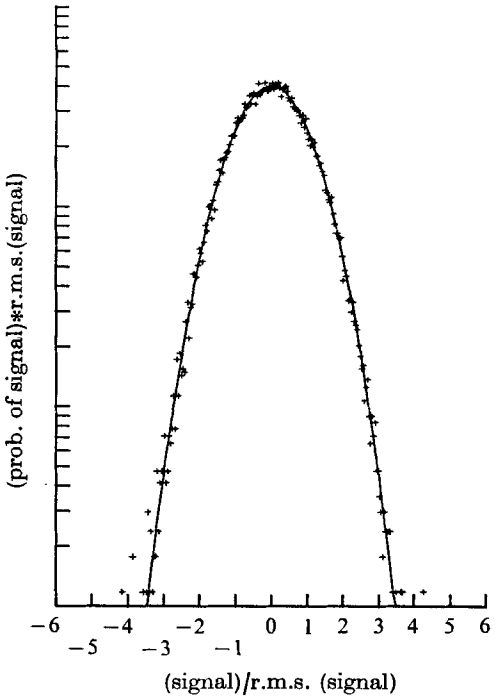

FIGURE 13. Probability density of filtered Fourier coefficients of Du/Dt for pipe flow. Bandwidth $1\Delta f$ (= 17·57 Hz).

7.2. *Fourth-cumulant spectrum*

In § 3 it was shown that the kurtosis of the narrow-band filtered coefficients is related to the fourth-order spectrum; the relation was given by (18); i.e.

$$\frac{1}{64}\frac{T[\kappa(\Delta\omega)-3]}{\pi[\kappa(\infty)-3]} \sim \frac{S_4(\omega)}{S_2^2(\omega)}.$$

$S_4(\omega)$ is a very special part of the fourth-order spectrum, defined by

$$S_4(\omega_1,\omega_2,\omega_3) = \frac{1}{(2\pi)^3}\iiint_{-\infty}^{+\infty} \exp\left[-i(\omega_1 x_1+\omega_2 x_2+\omega_3 x_3)\right]\mathscr{C}_4(\mathbf{x})\,d\mathbf{x}.$$

In order to comprehend more fully the quantity given by (18), we must write the left-hand side of (18), the kurtosis of narrow-band filtered Fourier coefficients, explicitly. As the bandwidth becomes small, this approaches

$$\begin{aligned}
&\overline{\left(\int_0^T u(t)\cos(\omega t)\,df\right)^4} - 3\overline{\left(\int_0^T u(t)\cos(\omega t)\,dt\right)^2}^2 + \overline{\left(\int_0^T u(t)\sin(\omega t)\,dt\right)^4}\\
&\quad - 3\overline{\left(\int_0^T u(t)\sin(\omega t)\,dt\right)^2}^2 \to 2^3\int_0^T dt\iiint_0^t \mathscr{C}_4(\mathbf{x})\cos[\omega(t-x_1)]\cos[\omega(t-x_2)]\\
&\quad\times\cos[\omega(t-x_3)]\cos(\omega t)\,dx_1\,dx_2\,dx_3 + 2^3\int_0^T dt\iiint_0^t \mathscr{C}_4(\mathbf{x})\sin[\omega(t-x_1)]\\
&\quad\times\sin[\omega(t-x_2)]\sin[\omega(t-x_3)]\sin(\omega t)\,dx_1\,dx_2\,dx_3, \qquad (21)
\end{aligned}$$

and $x_\alpha = t_\alpha - t_1$. It is of interest to find the relation between (21) and the experimentally-calculated kurtosis of the filtered Fourier coefficients.

Let C_t represent $\cos \omega t$; C_i and S_i be $\cos(\omega x_i)$, $\sin(\omega x_i)$, $i = 1, 2, 3$, respectively. Then the real part of the trigonometric term in (21) is

$$\begin{aligned}\text{trig} &= \cos[\omega(t-x_1)]\cos[\omega(t-x_2)]\cos[\omega(t-x_3)]\cos(\omega t)\\ &= (C_tC_1+S_tS_1)(C_tC_2+S_tS_2)(C_tC_3+S_tS_3)C_t,\end{aligned}$$

using trigonometric identities. Expanding,

$$\begin{aligned}\text{trig} &= [C_t^2C_1C_2+C_tS_t(C_1S_2+S_1C_2)+S_t^2S_1S_2](C_t^2C_3+C_tS_tS_3)\\ &= C_t^4C_1C_2C_3+C_t^2C_tS_t[C_3C_1S_2+C_3S_1C_2+S_3C_1C_2]\\ &\qquad +S_t^2C_tS_tS_1S_2S_3+C_t^2S_t^2[S_1S_2C_3+S_2S_3C_1+S_1S_3C_2]. \qquad (22)\end{aligned}$$

Using the double-angle formulae,

$$\cos(2t) = 2\cos^2 t - 1 \quad \text{and} \quad \cos t \sin t = \tfrac{1}{2}\sin(2t),$$

after collecting like terms the trigonometric term becomes

$$\begin{aligned}\text{trig} &= \tfrac{3}{8}C_1C_2C_3+\tfrac{1}{8}[S_1S_2C_3+S_2S_3C_1+S_1S_3C_2]\\ &\quad +\tfrac{1}{2}C_{2t}C_1C_2C_3-\tfrac{1}{8}C_{4t}[S_1S_2C_3+S_2S_3C_1+S_1S_3C_2-C_1C_2C_3]\\ &\quad +(\tfrac{1}{4}S_{2t}+\tfrac{1}{8}S_{4t})[C_3C_1S_2+C_3S_1C_2+S_3C_1C_2]\\ &\quad +(\tfrac{1}{4}S_{2t}-\tfrac{1}{8}S_{4t})S_1S_2S_3. \qquad (23)\end{aligned}$$

Now, integrating over x_1, x_2, x_3 as in (21),

$$\begin{aligned}2^3\int_0^T dt\iiint_0^t \mathscr{C}_4(\mathbf{x})\{&\tfrac{3}{8}C_1C_2C_3+\tfrac{1}{8}[S_1S_2C_3+S_2S_3C_1+S_1S_3C_2]\\ &+\tfrac{1}{2}C_{2t}C_1C_2C_3-\tfrac{1}{8}C_{4t}[S_1S_2C_3+S_2S_3C_1+S_1S_3C_2-C_1C_2C_3]\\ &+(\tfrac{1}{4}S_{2t}+\tfrac{1}{8}S_{4t})[C_3C_1S_2+C_3S_1C_2+S_3C_1C_2]\\ &+(\tfrac{1}{4}S_{2t}-\tfrac{1}{8}S_{4t})S_1S_2S_3\}\,dx_1\,dx_2\,dx_3. \qquad (24)\end{aligned}$$

Perform the same analysis on the sine coefficient in (21): i.e.

$$2^3\int_0^T dt\iiint_0^t \mathscr{C}_4(\mathbf{x})\sin[\omega(t-x_1)]\sin[\omega(t-x_2)]\sin[\omega(t-x_3)]\sin(\omega t)\,dx_1\,dx_2\,dx_3.$$

Then

$$\begin{aligned}2^3\int_0^T dt\iiint_0^t \{&\tfrac{3}{8}C_1C_2C_3+\tfrac{1}{8}[S_1S_2C_3+S_1S_3C_2+S_2S_3C_1]\\ &-\tfrac{1}{2}C_{2t}C_1C_2C_3+\tfrac{1}{8}C_{4t}[C_1C_2C_3-S_1S_2C_3+S_1S_3C_2+S_2S_3C_1]\\ &-(\tfrac{1}{4}S_{2t}-\tfrac{1}{8}S_{4t})[C_3C_1S_2+C_3C_2S_1+C_1C_2S_3]\\ &-(\tfrac{1}{4}S_{2t}+\tfrac{1}{8}S_{4t})S_1S_2S_3\}\,dx_1\,dx_2\,dx_3. \qquad (25)\end{aligned}$$

When we add (24) and (25), the terms involving C_{2t} or S_{2t} cancel. For the trigonometric part, we then have

$$\begin{aligned}&2\{(\tfrac{3}{8}+\tfrac{1}{8}C_{4t})C_1C_2C_3+\tfrac{1}{8}S_{4t}[C_1C_3S_2+C_3C_2S_1+C_1C_2S_3-S_1S_2S_3]\\ &\qquad +(\tfrac{1}{8}-\tfrac{1}{8}C_{4t})(S_1S_2C_3+S_2S_3C_1+S_1S_3C_2)\}\\ &= 2\{\tfrac{3}{8}C_1C_2C_3+\tfrac{1}{8}(C_1C_2C_3-C_{1+2+3})+\tfrac{1}{8}C_{4t}(C_{1+2+3})+\tfrac{1}{8}S_{4t}S_{1+2+3}\}\\ &= 2\{\tfrac{1}{2}C_1C_2C_3-\tfrac{1}{8}C_{1+2+3}+\tfrac{1}{8}C_{4t}C_{1+2+3}+\tfrac{1}{8}S_{4t}S_{1+2+3}\}\\ &= 2\{\tfrac{1}{2}C_1C_2C_3-\tfrac{1}{8}C_{1+2+3}+\tfrac{1}{8}C_{1+2+3-4t}\}. \qquad (26)\end{aligned}$$

Now, denote the real part of the filtered Fourier coefficients by A and the imaginary part by B. Then we can write (21) as

$$\tfrac{1}{2}(\overline{A^4}-\overline{3A^2}^2+\overline{B^4}-\overline{3B^2}^2)$$
$$\cong 2^3\int_0^T dt\iiint_0^t \mathscr{C}_4(\mathbf{x})\,[\tfrac{1}{2}C_1C_2C_3-\tfrac{1}{8}C_{1+2+3}+\tfrac{1}{8}C_{1+2+3-4t}]\,dx_1\,dx_2\,dx_3. \quad (27)$$

The final term is oscillatory in t; hence it will make a negligible contribution for large T. For more moderate values of T, however, it may be expected to slow the convergence.

One can easily obtain an expression in which it is not present. Let us form

$$\left(\int_0^T \exp(i\omega t)\,u(t)\,dt\right)^4-3\left(\int_0^T \exp(i\omega t)\,u(t)\,dt\right)^2$$
$$=\iiint\int_0^T \cos[\omega(t_1+t_2+t_3+t_4)]\,\mathscr{C}_4(\mathbf{t})\,d\mathbf{t}+i\iiint\int_0^T \sin[\omega(t_1+t_2+t_3+t_4)]\,\mathscr{C}_4(\mathbf{t})\,d\mathbf{t}.$$

This is symmetric under interchange of any two t_i. We now have

$$\overline{\left(\int_0^T \exp(i\omega t)\,u(t)\,dt\right)^4}-3\,\overline{\left(\int_0^T \exp(i\omega t)\,u(t)\,dt\right)^2}^2$$
$$\cong 2^3\int_0^T dt\iiint_0^t \cos[\omega(4t-x_1-x_2-x_3)]\,\mathscr{C}_4(\mathbf{x})\,d\mathbf{x}$$
$$+i2^3\int_0^T dt\iiint_0^t \sin[\omega(4t-x_1-x_2-x_3)]\,\mathscr{C}_4(\mathbf{x})\,d\mathbf{x}. \quad (28)$$

Here

$$t_1-t_2=x_1,\quad t_1+t_2+t_3+t_4=t_1+t_1-x_1+t_1-x_2+t_1-x_3=4t_1-x_1-x_2-x_3.$$

Thus, $C_{1+2+3-4t}$ results from the real part of (28). If we have a Fourier coefficient $A+iB$,

$$\overline{(A+iB)^4}-3\overline{(A+iB)^2}^2=\overline{A^4}+i4\overline{A^3B}-6\overline{A^2B^2}-i4\overline{AB^3}+\overline{B^4}-3(\overline{A^2}+2i\overline{AB}-\overline{B^2})^2.$$

Now, from (27),

$$\tfrac{1}{2}(\overline{A^4}-3\overline{A^2}^2+\overline{B^4}-3\overline{B^2}^2)-\tfrac{1}{8}\operatorname{Re}\left[\overline{\left(\int_0^T \exp(i\omega t)\,u(t)\,dt\right)^4}-3\,\overline{\left(\int_0^T \exp(i\omega t)\,u(t)\,dt\right)^2}^2\right]$$
$$=\tfrac{1}{2}(\overline{A^4}-3\overline{A^2}^2+\overline{B^4}-3\overline{B^2}^2)-\tfrac{1}{8}[\overline{A^4}-6\overline{A^2B^2}+\overline{B^4}-3(\overline{A^2}^2-4\overline{AB}^2+\overline{B^2}^2-2\overline{A^2}\,\overline{B^2})]$$
$$\cong 2^3T\iiint_{[C,1]}\int_0^\infty \mathscr{C}_4(\mathbf{x})\,[\tfrac{1}{2}C_1C_2C_3-\tfrac{1}{8}C_{1+2+3}]\,dx_1\,dx_2\,dx_3. \quad (29)$$

When we simplify the left-hand side of (29),

$$\tfrac{3}{8}(\overline{A^2+B^2})^2-\tfrac{9}{8}[(\overline{A^2}+\overline{B^2})^2+\tfrac{4}{3}(\overline{AB}^2-\overline{A^2}\,\overline{B^2})]. \quad (30)$$

This will approach most rapidly to

$$2^3T\left\{\frac{1}{2}\iiint_{[C,1]}\int_0^\infty \mathscr{C}_4(\mathbf{x})\cos(\omega x_1)\cos(\omega x_2)\cos(\omega x_3)\,d\mathbf{x}\right.$$
$$\left.-\frac{1}{8}\iiint_{[C,1]}\int_0^\infty \mathscr{C}_4(\mathbf{x})\cos[\omega(x_1+x_2+x_3)]\,d\mathbf{x}\right\}. \quad (31)$$

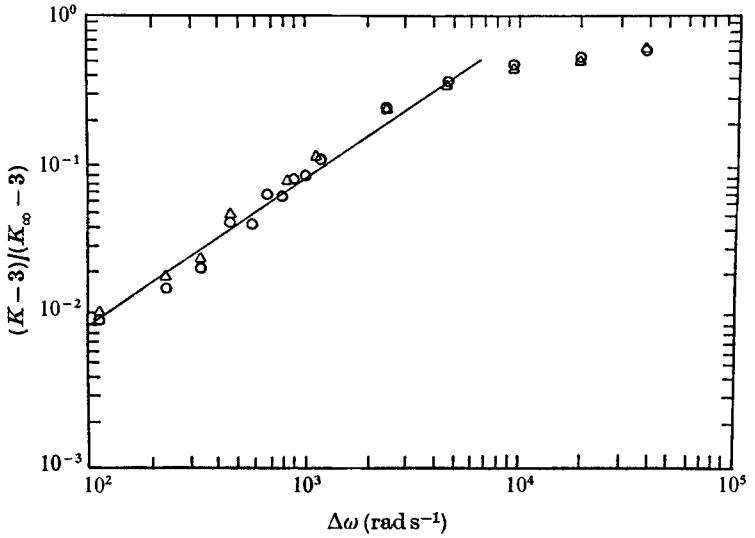

FIGURE 14. Kurtosis of narrow-band filtered velocity derivative for pipe flow. Comparison of two methods of calculation.

Expression (30) was calculated numerically. The results are shown in figure 14. The points marked by circles are the points transferred from figure 8, effectively quantity (27); the points marked by triangles are the numerical results of (30). The two practically coincide.

The purpose of using the more complicated expression (30) is to eliminate the extraneous time-dependent term in (21), improving convergence. (There are in general many expressions that approach the desired quantity, some faster than others, because slower converging terms cancel.) In our case, however, the records are evidently sufficiently long that there is virtually no difference between the results, and the more complicated expression is unnecessary.

One can also conclude (from figure 14) that $(K(\Delta\omega)-3)/(K(\infty)-3)$ approaches (31) as the bandwidth becomes small. The task is now to find what part of the fourth-order cumulant spectrum corresponds to (31). To do this, we must first examine the symmetry of the fourth-order cumulant spectrum.

The symmetry of the higher-order spectra is discussed exclusively by Brillinger & Rosenblatt (1967*b*). The fourth-order spectrum possesses a symmetry

$$\begin{aligned} S_4(\omega_1,\omega_2,\omega_3) &= S_4(\omega_2,\omega_1,\omega_3) = S_4(\omega_3,\omega_2,\omega_1) = S_4(\omega_1,\omega_3,\omega_2) \\ &= S_4(\omega_2,\omega_3,\omega_1) = S_4(\omega_3,\omega_1,\omega_2) = S_4(-\omega_1-\omega_2-\omega_3,\omega_2,\omega_3) \\ &= S_4(\omega_1,-\omega_2-\omega_3-\omega_1,\omega_3) = S_4(\omega_1,\omega_2,-\omega_3-\omega_1-\omega_2). \end{aligned} \tag{32}$$

Among the relations given in (32), only four are independent. They are

$$\begin{aligned} S_4(\omega_1,\omega_2,\omega_3) &= S_4(-\omega_1-\omega_2-\omega_3,\omega_2,\omega_3) \\ &= S_4(\omega_1,-\omega_2-\omega_1-\omega_3,\omega_3) = S_4(\omega_1,\omega_2,-\omega_3-\omega_1-\omega_2). \end{aligned} \tag{33}$$

If we write the symmetry relations in terms of the cumulant, they become

$$\begin{aligned} \mathscr{C}_4(x_1,x_2,x_3) &= \mathscr{C}_4(-x_1,x_2-x_1,x_3-x_1) = \mathscr{C}_4(x_1-x_2,-x_2,x_3-x_2) \\ &= \mathscr{C}_4(x_1-x_3,x_2-x_3,-x_3). \end{aligned} \tag{34}$$

Using this, the fourth-order spectrum can be written

$$S_4(\omega_1,\omega_2,\omega_3) = \iiint_{-\infty}^{+\infty} \exp\left[i(\omega_1 x_1+\omega_2 x_2+\omega_3 x_3)\right] \mathscr{C}_4(x_1,x_2,x_3)\,dx_1\,dx_2\,dx_3$$

$$= \iiint_0^{\infty} \{\exp\{i(\omega_1 x_1+\omega_2 x_2+\omega_3 x_3)\}$$
$$+\exp\{i[-\omega_1 x_1+\omega_2(x_2-x_1)+\omega_3(x_3-x_1)]\}$$
$$+\exp\{i[\omega_1(x_1-x_2)-\omega_2 x_2+\omega_3(x_3-x_2)]\}$$
$$+\exp\{i[\omega_1(x_1-x_3)+\omega_2(x_2-x_3)-\omega_3 x_3]\}\}$$
$$\times \mathscr{C}_4(x_1,x_2,x_3)\,dx_1\,dx_2\,dx_3. \quad (35)$$

The form of (35) is useful in finding the exact relation between (31) and the definition of the fourth-order spectrum. To simplify the algebra, let us denote $\cos(\omega x_i)$ and $\sin(\omega x_i)$ by C_i, S_i, respectively. The trigonometric part of (35) is

$$\text{trig} = \exp\{i(\omega_1 x_1+\omega_2 x_2+\omega_3 x_3)\}+\exp\{i[(-\omega_1-\omega_2-\omega_3)x_1+\omega_2 x_2+\omega_3 x_3]\}$$
$$+\exp\{i[\omega_1 x_1+(-\omega_2-\omega_1-\omega_3)x_2+\omega_3 x_3]\}$$
$$+\exp\{i[\omega_1 x_1+\omega_2 x_2+(-\omega_3-\omega_2-\omega_1)x_3]\}. \quad (36)$$

Let us investigate (36) for the cases

(i) $\omega_1=\omega_2=\omega_3=\omega$, (ii) $\omega_1=\omega_2=\omega_3=-\omega$,

(iii) $\omega_1=-\omega,\ \omega_2=\omega_3=\omega$, (iv) $\omega_1=\omega_3=\omega,\ \omega_2=-\omega$,

(v) $\omega_1=\omega_2=\omega,\ \omega_3=-\omega$, (vi) $\omega_1=\omega_2=-\omega,\ \omega_3=\omega$,

(vii) $\omega_1=\omega,\ \omega_2=\omega_3=-\omega$, (viii) $\omega_1=\omega_3=-\omega,\ \omega_2=\omega$.

(i) $\omega_1=\omega_2=\omega_3=\omega$. The trigonometric term (36) is first written in terms of sine and cosine.

$$\text{trig} = (C_1+iS_1)(C_2+iS_2)(C_3+iS_3)+(C_2+iS_2)(C_3+iS_3)(C_1-iS_1)^3$$
$$+(C_1+iS_1)(C_3+iS_3)(C_2+iS_2)^3+(C_1+iS_1)(C_2+iS_2)(C_3-iS_3)^3$$
$$= (C_1C_2-S_1S_2+iS_1C_2+iS_2C_1)(C_3+iS_3)$$
$$+(C_2C_3-S_2S_3+iS_2C_3+iS_3C_2)(C_1^3-i3C_1^2S_1-3C_1S_1^2+iS_1^3)$$
$$+(C_1C_3-S_1S_3+iS_1C_3+iS_3C_1)(C_2^3-i3C_2^2S_2-3C_2S_2^2+iS_2^3)$$
$$+(C_1C_2-S_1S_2+iS_1C_2+iS_2C_1)(C_3^3-i3C_3^2S_3-3C_3S_3^2+iS_3^3). \quad (37)$$

Using trigonometric relations, the real part of (37) reduces to

$$\text{Re(trig)} = 8C_1C_2C_3-4C_{1+2+3}-4S_1^2(C_1C_2C_3+C_3S_1S_2+C_2S_1S_3-C_1S_2S_3)$$
$$-4S_2^2(C_1C_2C_3+C_3S_1S_2-C_2S_1S_3+C_1S_2S_3)$$
$$-4S_3^2(C_1C_2C_3-C_3S_1S_2+C_2S_1S_3+C_1S_2S_3). \quad (38)$$

The first two terms of this form resemble (31), except for the coefficients. The trigonometric term in (31) is given by

$$\tfrac{1}{2}C_1C_2C_3-\tfrac{1}{8}C_{1+2+3}. \quad (39)$$

Evidently Re (trig) does not correspond to the quantity we calculated earlier.

(ii) $\omega_1 = \omega_2 = \omega_3 = -\omega$. This gives the same results as (38).

(iii) $\omega_1 = -\omega$, $\omega_2 = \omega_3 = \omega$.

$$\begin{aligned}\text{trig} &= \exp[i\omega(x_2+x_3-x_1)]+\exp[i\omega(x_2+x_3-x_1)]\\ &\quad+\exp[i\omega(x_3-x_1-x_2)]+\exp[i\omega(x_2-x_1-x_3)]\\ &= 2(C_2C_3+iC_2S_3+iC_3S_2-S_2S_3)(C_1-iS_1)\\ &\quad+(C_3C_1-iC_3S_1+iC_1S_3+S_1S_3)(C_2-iS_2)\\ &\quad+(C_2C_1-iC_2S_1+iC_1S_2+S_1S_2)(C_3-iS_3). \qquad (40)\end{aligned}$$

The real part of this is

$$\text{Re (trig)} = 4C_1C_2C_3+2(C_3S_1S_2+C_2S_1S_3).$$

In a similar manner,

(iv) $\omega_1 = \omega_3 = \omega$, $\omega_2 = -\omega$,

$$\text{Re (trig)} = 4C_1C_2C_3+2(C_1S_3S_2+C_3S_1S_2); \qquad (41)$$

(v) $\omega_1 = \omega_2 = \omega$, $\omega_3 = -\omega$,

$$\text{Re (trig)} = 4C_1C_2C_3+2(C_1S_2S_3+C_2S_1S_3); \qquad (42)$$

(vi) $\omega_1 = \omega_2 = -\omega$, $\omega_3 = \omega$,

$$\text{Re (trig)} = 4C_1C_2C_3+2(C_1S_3S_2+C_2S_1S_3); \qquad (43)$$

(vii) $\omega_1 = \omega$, $\omega_2 = \omega_3 = -\omega$,

$$\text{Re (trig)} = 4C_1C_2C_3+2(C_2S_1S_3+C_3S_1S_2); \qquad (44)$$

(viii) $\omega_1 = \omega_3 = -\omega$, $\omega_2 = \omega$,

$$\text{Re (trig)} = 4C_1C_2C_3+2(C_1S_2S_3+C_3S_1S_2). \qquad (45)$$

In (40)–(45), even though each term does not resemble the expression of (39), their combination might. Combining (40)–(45),

$$\begin{aligned}\sum_{\substack{\omega_1=\omega_2=-\omega_3=\pm\omega\\ \omega_1=-\omega_2=\omega_3=\pm\omega\\ -\omega_1=\omega_2=\omega_3=\pm\omega}}\text{Re (trig)} &= 24C_1C_2C_3+2(C_3S_1S_2+C_2S_1S_3)+2(C_1S_3S_2+C_3S_1S_2)\\ &\quad+2(C_1C_2C_3+C_2S_1S_3)+2(C_1S_3S_2+C_2S_1S_3)\\ &\quad+2(C_2S_1S_3+C_3S_1S_2)+2(C_1S_2S_3+C_3S_1S_2)\\ &= 24C_1C_2C_3+8(S_1S_2C_3+S_1C_2S_3+C_1S_2S_3). \qquad (46)\end{aligned}$$

Next we use

$$\begin{aligned}\cos\omega(x_1+x_2+x_3) &= \cos\omega x_1\cos\omega x_2\cos\omega x_3-\sin\omega x_1\sin\omega x_2\cos\omega x_3\\ &\quad-\sin\omega x_1\cos\omega x_2\sin\omega x_3-\cos\omega x_1\sin\omega x_2\sin\omega x_3,\end{aligned}$$

or

$$C_{1+2+3} = C_1C_2C_3-S_1S_2C_3-S_1C_2S_3-C_1S_2S_3.$$

Equation (46) becomes

$$\sum_{\substack{\omega_1=\omega_2=-\omega_3=\pm\omega\\ \omega_1=-\omega_2=\omega_3=\pm\omega\\ -\omega_1=\omega_2=\omega_3=\pm\omega}}\text{Re (trig)} = 32C_1C_2C_3-8C_{1+2+3}. \qquad (47)$$

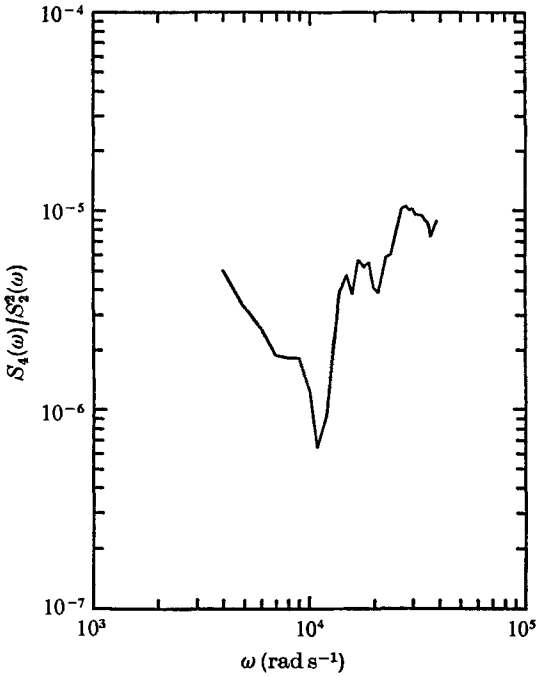

FIGURE 15. $S_4(\omega)/S_2^2(\omega)$ against frequency for pipe flow. Bandwidth $1\Delta f$ ($1\Delta f$ = 17·57 Hz).

If we divide both sides of (47) by 64,

$$\tfrac{1}{64} \sum_{\substack{\omega_1=\omega_2=-\omega_3=\pm\omega \\ \omega_1=-\omega_2=\omega_3=\pm\omega \\ -\omega_1=\omega_2=\omega_3=\pm\omega}} \mathrm{Re}\,(\mathrm{trig}) = \tfrac{1}{2}C_1C_2C_3 - \tfrac{1}{8}C_{1+2+3}. \tag{48}$$

This is identical to (39).

Thus, the coefficient of the excess of narrow-band filtered Fourier coefficients approaches what may be called the 'symmetric' part of the fourth-order spectrum (although, of course, with three variables there are many ways in which such might be defined). It is curious that (48) excludes, of the eight points in the frequency three-space of magnitude ω, the two in the principal diagonal at which the values are equal. That is,

$$\begin{aligned} S_4(\omega) = \tfrac{1}{64}[&S_4(-\omega,\omega,\omega)+S_4(\omega,-\omega,\omega)+S_4(\omega,\omega,-\omega) \\ &+S_4(-\omega,-\omega,\omega)+S_4(\omega,-\omega,-\omega)+S_4(-\omega,\omega,-\omega)]. \end{aligned} \tag{49}$$

The fourth-order cumulant spectrum given by (49) can be evaluated alternatively by calculating the quantity on the left-hand side of (18). Results are shown in figures 15–19 for pipe flow, and figures 20–25 for jet flow. The values of the normalized fourth-order spectrum $S_4(\omega)/S_2^2(\omega)$ at a particular ω correspond to that of kurtosis of the narrow-band filtered Fourier coefficient multiplied by a factor involving the filter bandwidth. The exact relation is given by (18), or

$$\frac{1}{64}\frac{T}{\pi}\left[\frac{K(\Delta\omega)-3}{K(\infty)-3}\right].$$

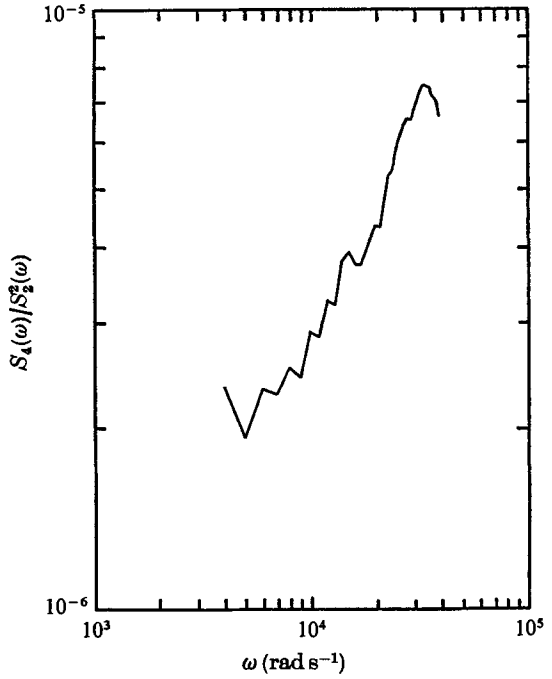

FIGURE 16. $S_4(\omega)/S_2^2(\omega)$ against frequency for pipe flow. Bandwidth $3\Delta f$ ($1\Delta f$ = 17·57 Hz).

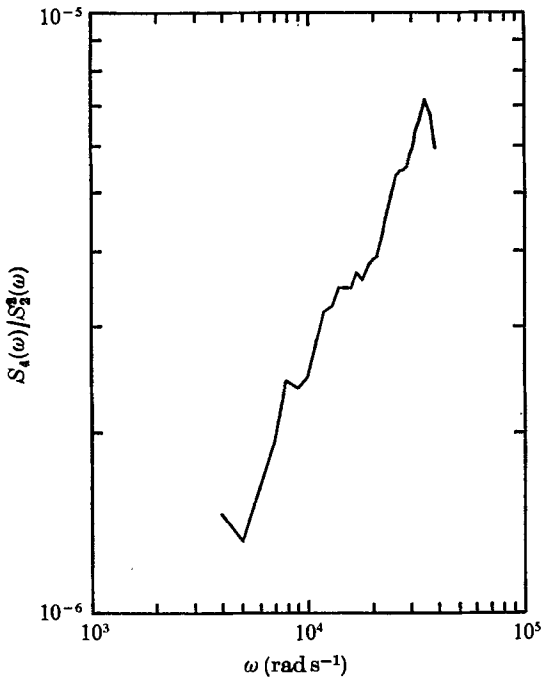

FIGURE 17. $S_4(\omega)/S_2^2(\omega)$ against frequency for pipe flow. Bandwidth $5\Delta f$ ($1\Delta f$ = 17·57 Hz).

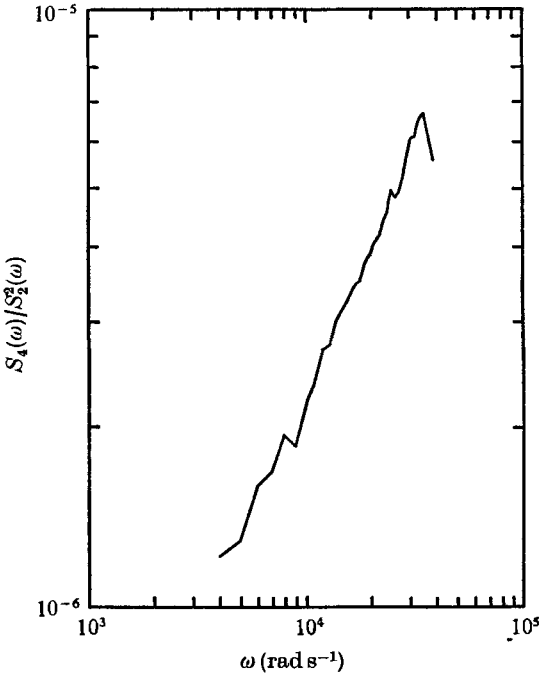

FIGURE 18. $S_4(\omega)/S_2^2(\omega)$ against frequency for pipe flow. Bandwidth $7\Delta f$ ($1\Delta f = 17{\cdot}57$ Hz).

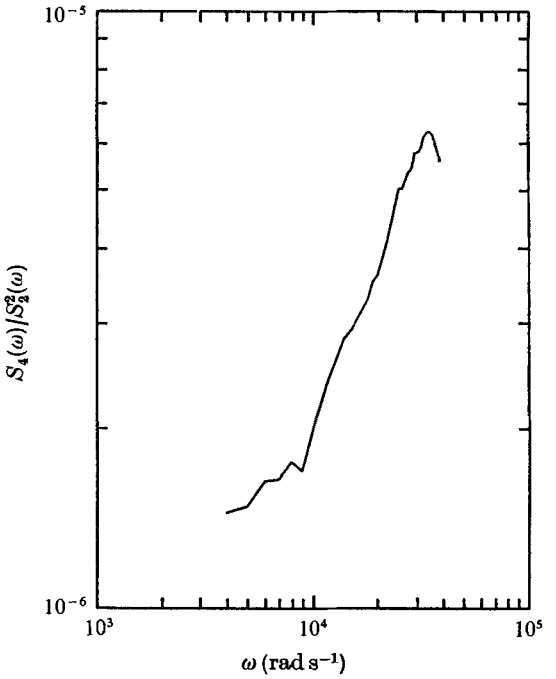

FIGURE 19. $S_4(\omega)/S_2^2(\omega)$ against frequency for pipe flow. Bandwidth $9\Delta f$ ($1\Delta f = 17{\cdot}57$ Hz).

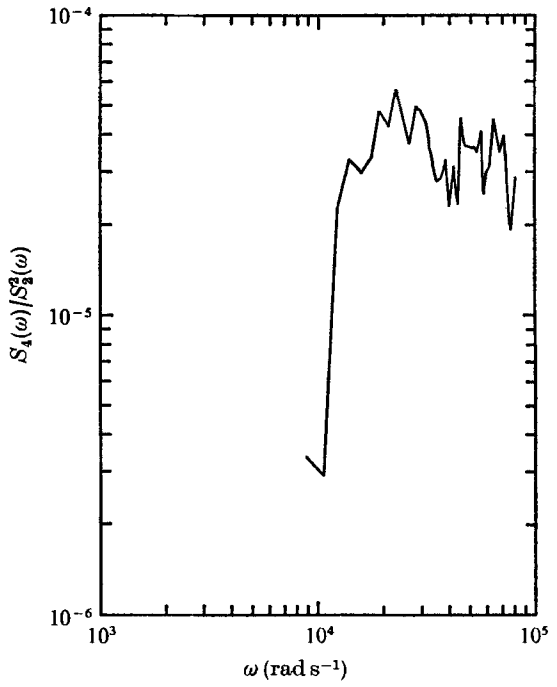

FIGURE 20. $S_4(\omega)/S_2^2(\omega)$ against frequency for jet flow. Bandwidth $1\Delta f$ ($1\Delta f$ = 4·39 Hz).

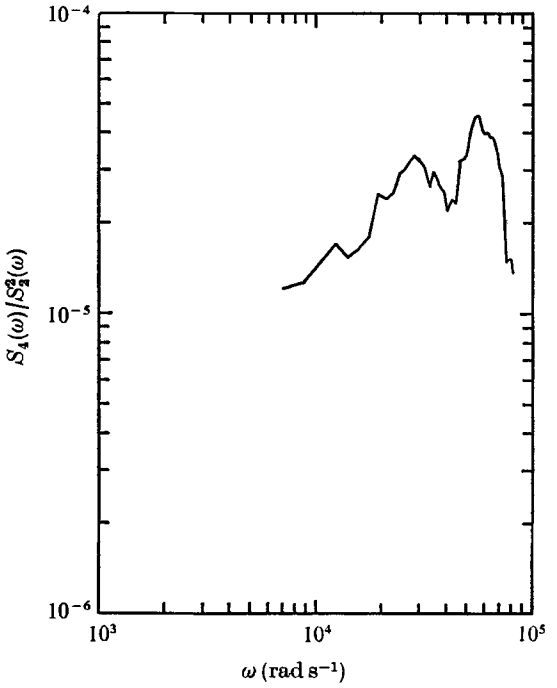

FIGURE 21. $S_4(\omega)/S_2^2(\omega)$ against frequency for jet flow. Bandwidth $2\Delta f$ ($1\Delta f$ = 4·39 Hz).

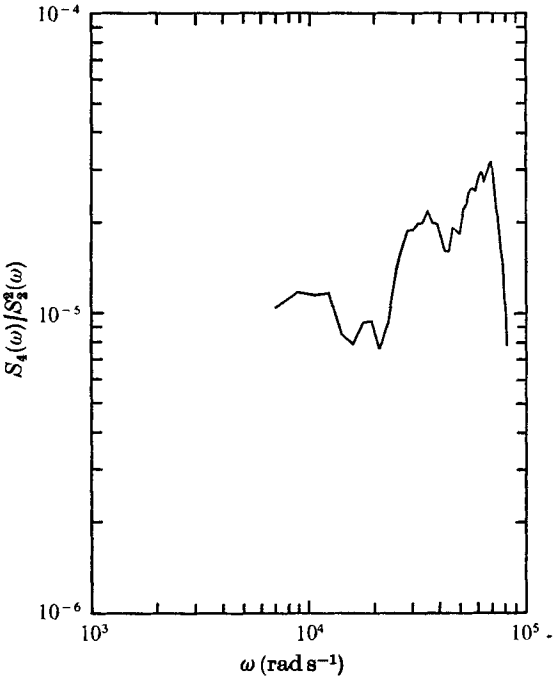

FIGURE 22. $S_4(\omega)/S_2^2(\omega)$ against frequency for jet flow. Bandwidth $4\Delta f$ ($1\Delta f$ = 4·39 Hz).

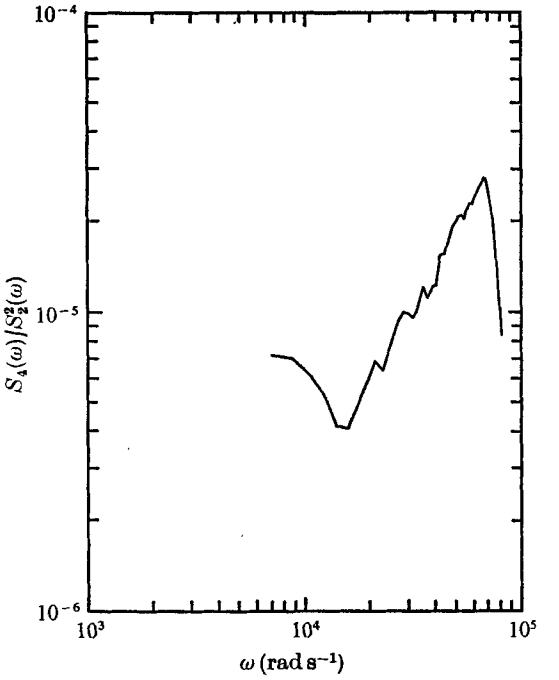

FIGURE 23. $S_4(\omega)/S_2^2(\omega)$ against frequency for jet flow. Bandwidth $8\Delta f$ ($1\Delta f$ = 4·39 Hz).

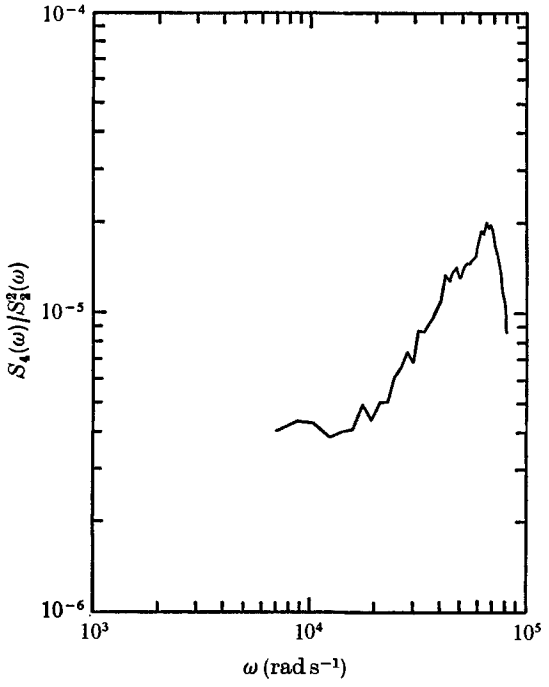

FIGURE 24. $S_4(\omega)/S_2^2(\omega)$ against frequency for jet flow. Bandwidth $16\Delta f$ ($1\Delta f = 4{\cdot}39$ Hz).

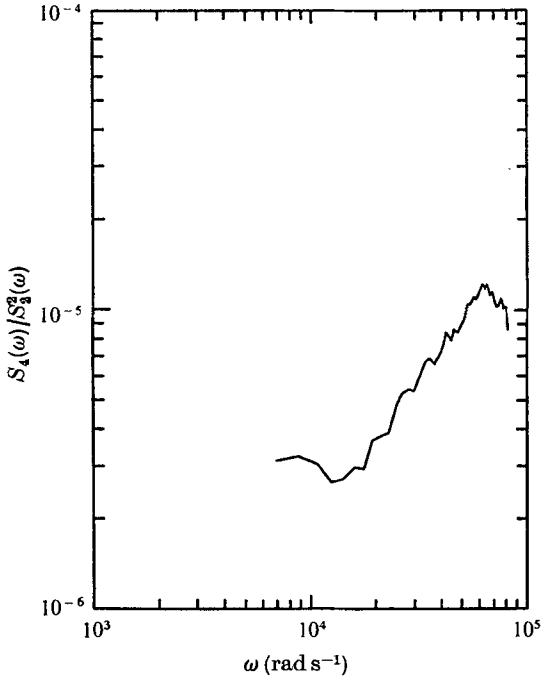

FIGURE 25. $S_4(\omega)/S_2^2(\omega)$ against frequency for jet flow. Bandwidth $32\Delta f$ ($1\Delta f = 4{\cdot}39$ Hz).

For example, for pipe flow, the values of kurtosis shown in figure 8 for each bandwidth were obtained with the centre-frequency fixed at $f_0 = 3{\cdot}00\,\text{kHz}$ or $\omega_0 = 18\,868$, which corresponds to $64\pi/T$ times $S_4(18\,877)/S_2^2(18\,877)$, shown in figures 15–19 for each bandwidth. For jet flow, the centre-frequency was fixed at 5·8 kHz. Here T is $(\Delta f')^{-1}$. ($\Delta f'$ is the width of the filter.) The normalized fourth-order spectra, shown in figures 15–25, are the results of smoothed spectra, obtained by a moving-average technique. Thus, comparing the values of kurtosis shown in figure 8 with those of $S_4(\omega_0)/S_2^2(\omega_0)$, the latter gives only an average value in the neighbourhood of the centre-frequency, not an exact value, as does the former.

This shows that the relative value of the fourth-order spectrum increases with frequency. The peak of all the curves occurs approximately at the frequency corresponding to unity signal-to-noise ratio of the second-order spectrum. Since the values of $S_4(\omega)/S_2^2(\omega)$, shown in figures 15–19, are a measure of intrinsic excess, the increase of $S_4(\omega)/S_2^2(\omega)$ with frequency implies that higher excess is associated with smaller scales of the flow (high wavenumber). We have no definite explanation of why the curves appear to have a nearly constant slope. It seems likely that it could be predicted using one of the models proposed by e.g. Novikov & Stewart (1964) and Novikov (1965, 1966). In these, it is supposed (in agreement with observation) that the non-Gaussian behaviour of the small scales arises from intermittency. That is, if a region is divided into sub-regions, each of which is again sub-divided in the same way, relatively few sub-regions contain much small-scale energy, and this is true for each sub-division. The kurtosis (and higher moments) can thus (in principle) be expressed in terms of the intermittency. Since S_4/S_2^2 is the *intrinsic* excess (i.e. that per unit wavenumber), this too should be expressible. Some of the models are fairly explicitly multiplicative, with successive factors obeying similarity relations. Various attempts were made to predict the behaviour of S_4/S_2^2 on the basis of these, without success.

Except at very small filter bandwidth, the slopes of these curves are approximately equal. At the small filter bandwidth, the lack of data record length causes the values to fluctuate considerably, and fail to attain statistical stability. As the filter bandwidth increases, more coefficients being summed together, the statistics improve, and the values show a definite variation with frequency. This suggests that, at the small filter bandwidth, the calculated value of $S_4(\omega)/S_2^2(\omega)$ is unreliable. Thus, it is necessary to find an appropriate method to predict an experimental asymptotic value for vanishing filter bandwidth.

Suppose A_T is the Fourier coefficient corresponding to integration time T, and n the number of records of data. One writes the averaged value

$$\widetilde{A_T^4} = \frac{1}{n}\sum_1^n A_T^4, \quad \widetilde{A_T^2} = \frac{1}{n}\sum_1^n A_T^2. \tag{50}$$

Then the uncertainty from the true ensemble-averaged value $\overline{A_T^4}$ is

$$\epsilon_4 = \frac{\frac{1}{n}\sum_1^n A_T^4 - \overline{A_T^4}}{\overline{A_T^4}}, \quad \epsilon_2 = \frac{\frac{1}{n}\sum_1^n A_T^2 - \overline{A_T^2}}{\overline{A_T^2}}, \tag{51}$$

where $\overline{\epsilon_4} = \overline{\epsilon_2} = 0$. For a Gaussian variable, $\overline{\epsilon_4^2} = 32/3n$ and $\overline{\epsilon_2^2} = 2/n$. As a matter of fact, our previous results indicate that, for long time T, A_T is nearly Gaussian, and furthermore ϵ_2 and ϵ_4 will be only weakly dependent on T. For a particular set of n records, ϵ_2 and ϵ_4 have a fixed value.

Using the fact that $\epsilon_2 \ll 1$, the experimentally-averaged fourth moments can be written

$$\frac{\widetilde{A_T^4} - 3\widetilde{A_T^2}^2}{\widetilde{A_T^2}^2} \cong \frac{\overline{A_T^4} - 3\overline{A_T^2}^2}{\overline{A_T^2}^2}(1-2\epsilon_2) + \frac{\overline{A_T^4}\epsilon_4 - 6\overline{A_T^2}^2\epsilon_2}{\overline{A_T^2}^2}. \tag{52}$$

Using the fact that A_T is nearly Gaussian, (52) becomes

$$\frac{\widetilde{A_T^4} - 3\widetilde{A_T^2}^2}{\widetilde{A_T^2}^2} \cong \frac{\overline{A_T^4} - 3\overline{A_T^2}^2}{\overline{A_T^2}^2} + (3\epsilon_4 - 6\epsilon_2) = \frac{\overline{A_T^4} - 3\overline{A_T^2}^2}{\overline{A_T^2}^2} + \eta. \tag{53}$$

One can calculate $\overline{\eta^2}$ assuming Gaussian behaviour

$$\overline{\eta^2} = (3\epsilon_4 - 6\epsilon_2)^2 = 24/n. \tag{54}$$

This is essentially equivalent to the error involved in the calculation of the fourth moments of the filtered Fourier coefficients. According to (54), the uncertainty in jet flow becomes $(\overline{\eta^2})^{\frac{1}{2}} \sim 14{\cdot}7\,\%$ and for pipe flow $(\overline{\eta^2})^{\frac{1}{2}} \sim 3{\cdot}46\,\%$.

Now, for fixed n, as T increases, asymptotic analysis indicates that the first term of (53) behaves like

$$a/T - b/T^3 + \ldots. \tag{55}$$

The second term is essentially constant. Multiplying by T, we have

$$T(\widetilde{A_T^4} - 3\widetilde{A_T^2}^2)/\widetilde{A_T^2}^2 \cong a - b/T^2 + \eta T. \tag{56}$$

If we plot (56) in terms of T^{-1}, for small T^{-1} the third term ηT becomes dominant; and as T^{-1} increases the first two terms become dominant. In figure 26, the numerical results of the left-hand side of (56) for jet data are presented. The values plotted were normalized by $S_4(\omega)/S_2^2(\omega)$ at a bandwidth of $64\Delta f$ or ω of $1766{\cdot}4\,\mathrm{rad\,s^{-1}}$. At each bandwidth, statistics on the value of $S_4(\omega)/S_2^2(\omega)$ were gathered, to find the mean and the standard deviation. The circles in figure 26 correspond to the mean values; and the standard deviation at each bandwidth is indicated by a line at both sides of the mean value. The curve ηT was calculated using the value of η found from (54) for the jet data. η was found to be 0·147 for this case. The agreement of the analytical prediction with the experimental result is good, considering the experimental accuracy.

The true asymptotic value a may be found from the experimental values of $S_4(\omega)/S_2^2(\omega)$ through (56), by picking the value of T, say T_+, where the second derivative vanishes. Let

$$f(T^{-1}) = a - \frac{b}{T^2} + \eta T, \quad f' = -2bT^{-1} - \frac{\eta}{(T^{-1})^2},$$

$$f'' = -2b + \frac{2\eta}{(T^{-1})^3} = 0, \quad b = \frac{\eta}{(T^{-1})^3},$$

or

$$f(T_+^{-1}) = a - b(T_+^{-1})^2 + \eta/T_+^{-1} = a. \tag{57}$$

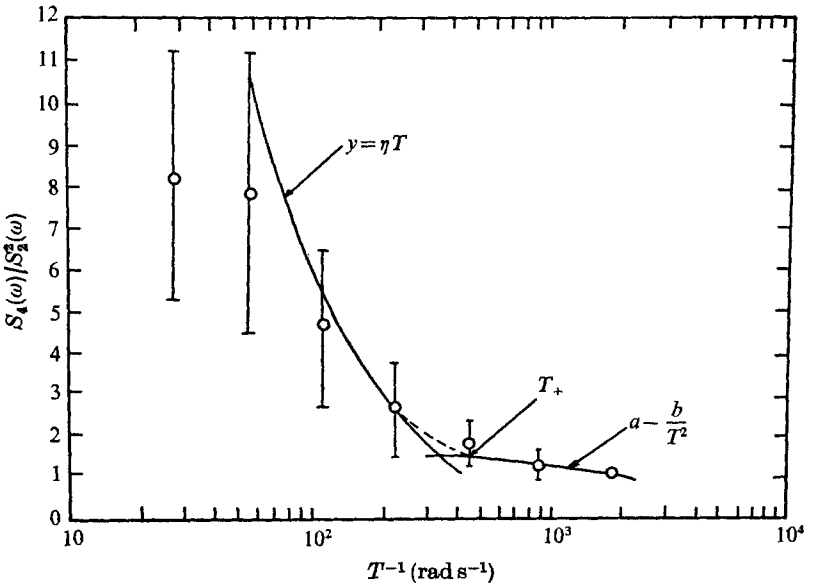

FIGURE 26. Experimental and analytical behaviour of (56).

The location of T_+ is also indicated in figure 26. The corresponding bandwidth is found to be $16\Delta f$ or 70·5 Hz, and at this bandwidth the corresponding asymptotic value is found to be $5{\cdot}5 \times 10^{-6}$. These results explain the erratic behaviour of the calculated values at small bandwidth: the relevant bandwidth in determining the asymptotic value is not the smallest, because of the uncertainty in the calculation. Thus, for jet data, the curves for bandwidths less than $16\Delta f$ should be ignored.

For jet flow, the bandwidth of $16\Delta f$ was chosen, to re-examine the fourth-order spectrum. The fourth-order spectrum densities corresponding to smaller frequencies at this bandwidth were also recalculated. Results are shown in figure 27. The fourth-order spectral densities stay approximately constant for the lower frequency range, before they exhibit any definite trend. We believe this to be because of the statistical accuracy limit in the calculation of $S_4(\omega)/S_2^2(\omega)$. From (18),

$$\frac{S_4(\omega)}{S_2^2(\omega)} \sim \frac{1}{64}\frac{T}{\pi}\frac{[K(\Delta\omega)-3]}{[K(\infty)-3]}.$$

To estimate the error in the calculation, let

$$\phi = S_4(\omega)/S_2^2(\omega).$$

Then, from (53),

$$\frac{1}{64}\frac{T}{\pi(K_\infty-3)}(K_T-3+\eta) = \phi,$$

where K_T is the true value. The error associated with ϕ is

$$\epsilon_\phi = \frac{1}{64}\frac{T}{\pi(K_\infty-3)}\eta. \tag{58}$$

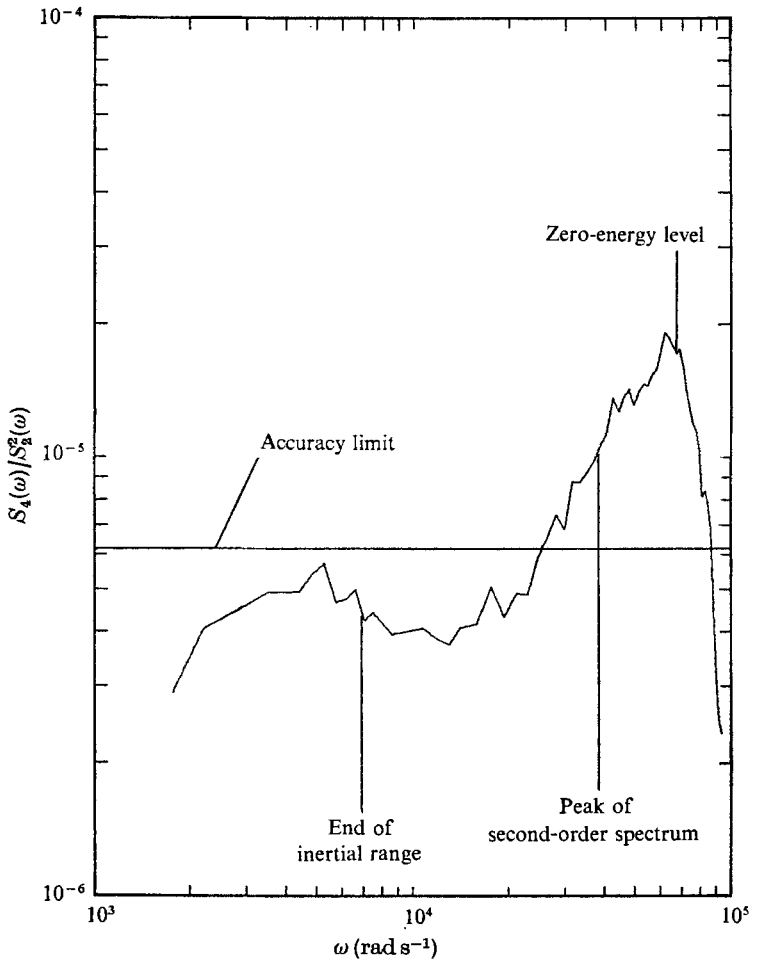

FIGURE 27. Fourth-order spectrum. Bandwidth = $16\Delta f$.

For $n = 1250$, $K_\infty - 3 = 3{\cdot}2$. Using $\eta^2 = 24/n$,

$$(\overline{\epsilon_\phi^2})^{\frac{1}{2}} = 3{\cdot}05 \times 10^{-6}. \tag{59}$$

From (53), it can be seen that the calculated value of the fourth moment is the sum of the true value and the uncertainty of the calculation. The values shown in figure 27 are the result of these sums; and the true values can be obtained by subtracting the uncertainty from them. Figure 28 represents the result of doing this. The accuracy limit in the calculation given by (59) is shown in figure 28. This is also indicated in figure 27, suggesting that the constant values of $S_4(\omega)/S_2^2(\omega)$ in this figure are an artifact of the computational inaccuracy.

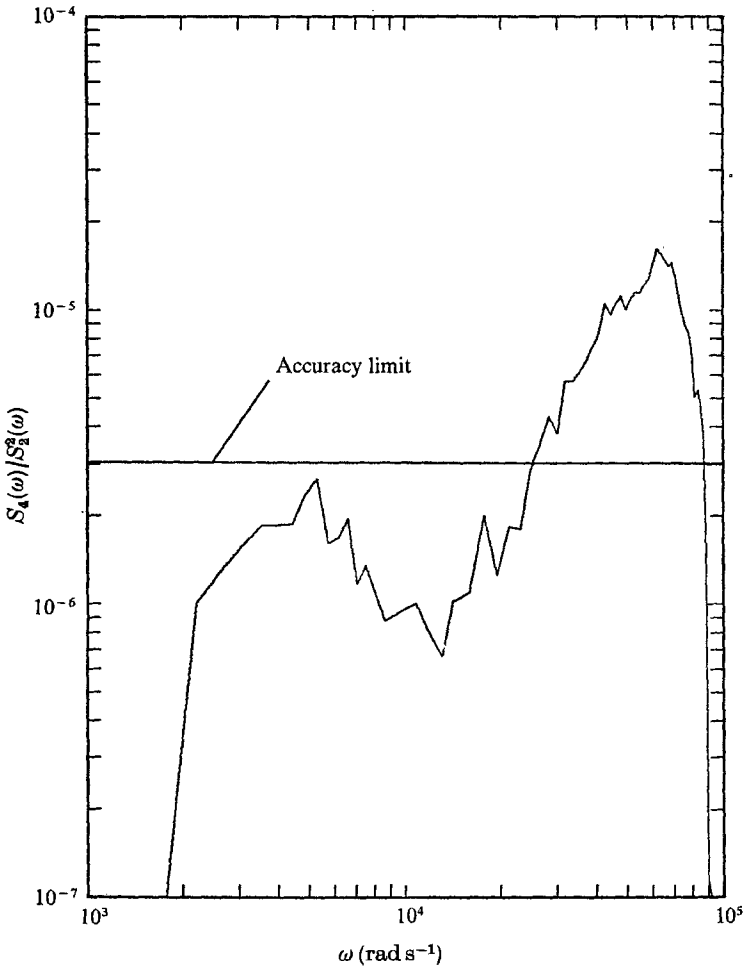

FIGURE 28. True experimental value of $S_4(\omega)/S_2^2(\omega)$ for jet flow. Bandwidth = $16\Delta f$.

8. Conclusions

8.1. *The central-limit theorem*

The experimental results shown in figures 7 and 8, and 9–13, completely support the analytical conclusion of Lumley (1971). The narrow-band filtered Fourier coefficients of non-Gaussian turbulent velocity derivative signals approach Gaussian as the filter bandwidth becomes small, and the rate of approach is proportional to the reciprocal of the filter bandwidth.

To demonstrate the approach to a Gaussian distribution of the velocity derivative signals experimentally, the product $\Delta f \mathscr{T}_u$ must be quite small. (Δf is the filter bandwidth; and $\mathscr{T}_u$ is the integral scale associated with the velocity signals.) Typically, it is order 5×10^{-2}. In addition, a sufficiently long total record of data is required to obtain good results. If a longer total is available, it is possible to improve the results of calculation by further reducing the bandwidth Δf.

8.2. *Higher-order spectra*

Define the fourth-order cumulant spectrum by

$$S_4(\omega_1,\omega_2,\omega_3)=\frac{1}{(2\pi)^3}\iiint_{-\infty}^{+\infty}\exp\left[-i(\omega_1x_1+\omega_2x_2+\omega_3x_3)\right]\mathscr{C}_4(x_1,x_2,x_3)\,dx_1\,dx_2\,dx_3. \tag{60}$$

($\mathscr{C}_4(x_1,x_2,x_3)$ is the fourth-order cumulant.) Then the kurtosis of narrow-band filtered Fourier coefficients for turbulence velocity derivative signals is related to a special part of the fourth-order cumulant spectrum. If the latter is denoted by $S_4(\omega)$, the relation is

$$\frac{1}{64}\frac{T(K(\Delta\omega)-3)}{\pi(K(\infty)-3)}\sim\frac{S_4(\omega)}{S_2^2(\omega)}. \tag{61}$$

Here,
$$\begin{aligned}S_4(\omega)&=\frac{1}{(2\pi)^3}\left[\frac{1}{2}\iiint_0^\infty\mathscr{C}_4(\mathbf{x})\cos\omega x_1\cos\omega x_2\cos\omega x_3\,d\mathbf{x}\right.\\&\quad\left.-\frac{1}{8}\iiint_0^\infty\mathscr{C}_4(\mathbf{x})\cos\omega(x_1+x_2+x_3)\,d\mathbf{x}\right]\\&=\tfrac{1}{64}[S_4(-\omega,\omega,\omega)+S_4(\omega,-\omega,\omega)+S_4(\omega,\omega,-\omega)\\&\quad+S_4(-\omega,-\omega,\omega)+S_4(\omega,-\omega,-\omega)+S_4(-\omega,\omega,-\omega)].\end{aligned} \tag{62}$$

The numerical calculation of $S_4(\omega)/S_2(\omega)$ showed that the fourth-order spectrum increases with frequency, with a nearly constant slope. An error analysis indicated that there is an optimum bandwidth for calculation of $S_4(\omega)/S_2^2(\omega)$, and that below this the calculated values become progressively less reliable.

This work was supported by the Atmospheric Science Section of the National Science Foundation under grant GA-35422X, and is based in part on the Ph.D. thesis of K.T. At the time of writing, J.L.L. was on leave as a Fulbright Senior Lecturer, Service of Professor J.C.J. Nihoul, Institute of Mathematics, University of Liège, Belgium.

REFERENCES

Batchelor, G. K. 1953 *The Theory of Homogeneous Turbulence.* Cambridge University Press.

Brillinger, D. R. & Rosenblatt, M. 1967*a* Asymptotic theory of estimates of Kth-order spectra. *Advanced Seminar on Spectral Analysis of Time Series* (ed. B. Harris). Wiley.

Brillinger, D. R. & Rosenblatt, M. 1967*b* Computation and interpretation of Kth-order spectra. *Advanced Seminar on Spectral Analysis of Time Series* (ed. B. Harris). Wiley.

Frenkiel, F. N. & Klebanoff, P. S. 1967 Higher-order correlations in a turbulent field. *Phys. Fluids*, **10**, 507.

Hasselman, K., Munk, W. & MacDonald, G. 1963 Bispectrum of ocean waves. *Time Series Analysis* (ed. M. Rosenblatt). Wiley.

Kraichnan, R. H. 1959 The structure of isotropic turbulence at very high Reynolds numbers. *J. Fluid Mech.* **5**, 497.

LUMLEY, J. L. 1970 *Stochastic Tools in Turbulence.* Academic.

LUMLEY, J. L. 1971 Application of central-limit theorems to turbulence problems. *Statistical Models and Turbulence, Lecture Notes in Physics*, vol. 12 (eds M. Rosenblatt & C. Van Atta). Springer.

LUMLEY, J. L. & WYNGAARD, J. C. 1967 A constant-temperature hot-wire anemometer. *J. Sci. Instr.* **44**, 363.

NILSEN, A. W. 1969 Analysis of the unsteady pressure in a turbulent jet. M.S. thesis, The Pennsylvania State University.

NOVIKOV, E. A. 1965 Higher-order correlations in turbulent flow. *Izv. Atmos. Ocean Phys.* **1**, 788.

NOVIKOV, E. A. 1966 Mathematical model for the intermittence of turbulent flow. *Soviet Phys. Doklady*, **11**, 497.

NOVIKOV, E. A. & STEWART, R. W. 1964 The intermittency of turbulence and the spectrum of energy dissipation fluctuations. *Izv. Atmos. Ocean Phys.* **3**, 408.

ROSENBLATT, M. 1956 A central limit theorem and a strong mixing condition. *Proc. Nat. Acad. Sci., U.S.A.* **42**, 43–47.

ROSENBLATT, M. 1961 Some comments on narrow-band pass filters. *Quart. Appl. Math.* **18**, 387.

ROSENBLATT, M. 1966 Remarks on higher-order spectra. *Symp. on Multivariate Analysis.* Academic.

ROSENBLATT, M. & VAN NESS, X. 1965 Estimation of the bispectrum. *Ann. Math. Stat.* **36**, 1120.

TAKEUCHI, K. & LUMLEY, J. L. 1976 On the kurtosis of wind velocity derivatives in atmospheric boundary layers. (To be submitted for publication.)

TENNEKES, H. & LUMLEY, J. L. 1972 *A First Course in Turbulence.* MIT Press.

VON FRANK, E. D. 1970 Turbulence characteristics in the mixing region of a perturbed and unperturbed round free jet. M.S. thesis, The Pennsylvania State University.

WYNGAARD, J. C. & LUMLEY, J. L. 1967 A sharp cutoff spectral differentiator. *J. Appl. Meteor.* **6**, 592.

YEH, T. T. & VAN ATTA, C. W. 1973 Spectral transfer of scalar and velocity fields in heated-grid turbulence. *J. Fluid Mech.* **58**, 233.